12-2000

Flow Near Submarine Canyons Driven by Constant Winds

Jun She
Old Dominion University

John M. Klinck
Old Dominion University, jklinck@odu.edu

Flow near submarine canyons driven by constant winds

Jun She[1] and John M. Klinck

Center for Coastal Physical Oceanography, Old Dominion University, Norfolk, Virginia

Abstract. Circulation over coastal submarine canyons driven by constant upwelling or downwelling wind stress is simulated and analyzed with a primitive equation ocean model. Astoria Canyon, on the west coast of North America, is the focus of this study, and model results are consistent with most major features of mean canyon circulation observed in Astoria Canyon. Near-surface flow crosses over the canyon, while a closed cyclone occurs within the canyon. Upwelling prevails within the canyon and is larger than wind-driven upwelling along the adjacent shelf break. Water rises from depths reaching 300 m to the canyon rim and, subsequently, onto the adjacent shelf. Onshore flow within the canyon is driven by the onshore pressure gradient force, due to the free surface slope created by the upwelling wind, and is enhanced by the limitation to alongshore flow by the canyon topography. Density gradients largely compensate the surface slope with realistic stratification, but continual upwelling persists near the edges of the canyon. Within the upper canyon (50-150 m below the canyon rim) a cyclone is created by flow turning into the canyon mouth, separating from the upstream edge, and advecting toward the downstream rim. Below this layer the cyclone is created by vortex stretching due to the upwelling. Downwelling winds create nearly the opposite flow, in which compression and momentum advection create a strong anticyclone within the canyon. Momentum advection is found to be important both in creating strong circulation within the canyon and in allowing the surface flow to cross the canyon undisturbed. Model results indicate that Astoria-like submarine canyons produce across shore transport of sufficient volume to flush a continental shelf in a few (2-5) years.

1. Introduction

Submarine canyons incise the shelf edge along most of the world's coastline and are important passages for across shore transport of nutrient-rich dense water and sediments [*Inman et al.*, 1976]. As a specific example of canyon-related upwelling, *Freeland and Denman* [1982] found a persistent pool of dense water on the shelf near Vancouver Island. Analysis of water properties indicated that it had come from offshore and depths of more than 400 m.

The circulation within and near canyons is complicated by interaction of stratified coastal flow and canyon topography. One of the best measured submarine canyons is Astoria, on the northwestern coast of North America [*Hickey*, 1997]. During northerly winds, upwelling prevails throughout the canyon, while a cyclone is found within the canyon and sometimes up to

[1]Now at Danish Meteorological Institute, Copenhagen, Denmark

50 m above the canyon rim [*Hickey*, 1997]. Water column stretching was observed within the canyon with vortex compression in a 50 m thick layer above the canyon. The upper layer of water over the shelf (100 m above the rim) is little influenced by the canyon topography.

Literature on theoretical analysis and modeling studies of canyon circulation is relatively sparse. *Freeland and Denman* [1982] proposed that the up-canyon flow was driven by the onshore geostrophic pressure gradient. *Klinck* [1988] discussed the effects of different canyon widths and suggested that a narrow canyon should be defined as one whose width is smaller than half of the internal Rossby deformation radius. Only a narrow canyon has a strong effect on the circulation, while a wide canyon just distorts flow to be along isobaths. With an analytical model, *Klinck* [1989] investigated the geostrophic adjustment over different canyon scales and examined the effects of canyon width on the canyon and coastal flow.

Klinck [1996] used a numerical model to simulate weakly and strongly stratified flow in both directions along the coast interacting with canyon topography. He found that the strength of stratification influences the magnitude of the topographic effect on coastal flow,

while the direction of incident flow has a much stronger effect on canyon-coast flow interaction. Right bounded flow (coast is to the right looking in the direction of flow) was largely benign with water rounding the canyon but otherwise not being much affected. Left bounded flow resulted in upwelling in the canyon and considerable transport of water across the shelf break.

Allen [1996] investigated the spin-up and steady state of narrow canyon circulation with analytical and numerical solutions of a three-layer model. Analytical solutions were obtained for the initial circulation and for steady state. These solutions display the deflection of the flow around the canyon in both layers over the shelf. The middle layer has considerable onshore flow over the canyon. Numerical solutions with and without momentum advection have similar flow patterns, but the steady solutions were markedly different. In particular, the cyclone in the canyon was associated with nonlinear advection as the flow turns into the canyon. This study shows that the onshore flow in the canyon under upwelling forcing is up to 50 times that which occurs over the shelf break. S. E. Allen (personal communication, 1998) likes to say, "Canyons steal coastal upwelling."

Both of theses studies [*Klinck*, 1996; *Allen*, 1996] show some similarity to observed canyon flow. Both models show upwelling and cyclonic vorticity in part of the canyon. Below the canyon rim, alongshore flow turns into the canyon, on the upstream side by *Klinck* [1996] and on the downstream side by *Allen* [1996]. Allen also finds that incident flow in the upper layer (to depths of 50 m) is not influenced by the canyon topography.

However, neither study included explicit wind forcing, and both models had simplified physics. Neither study showed the closed cyclonic streamlines in and near the canyon, nor was there upwelling over the entire canyon. Therefore neither model provides an explanation for a mean cyclonic circulation within the canyon.

Interaction of alongshore flow with canyon topography is time-dependent as *Hickey* [1997] showed in Astoria Canyon. Fluctuations of velocity, vorticity, and temperature have complicated phase relationships with each other and with the wind. None of these features have been simulated by the above mentioned models, so the physical processes associated with these observations have yet to be investigated.

This study has three purposes: (1) to demonstrate the capability of the coastal numerical model to simulate circulation in a generic narrow canyon, for both steady and transient forcing; (2) to improve our understanding of the mechanism of canyon circulation and its temporal variability; and (3) to extend observational results to other canyons. Discrepancies between the previous model studies and observations are considerable. It is clearly necessary to show the ability of a model to

simulate the main observational findings before analysis of mechanisms and calculation of cross-shelf flux is possible. This is our first objective.

Since there are constraints both in observation and modeling of canyon circulation, our understanding of the physics of canyon circulation is still limited. The second objective is to use the model to analyze both steady and transient processes. The major questions for steady flow include What produces the trapped cyclone within a narrow canyon; What are the roles of wind forcing, stratification, and nonlinearity; and What is the vertical excursion of water moving from the canyon onto the shelf? Transient flow situations raise additional questions How does the circulation change as the forcing changes; What is the phase relationship among vertical speed, vorticity, and temperature as the forcing changes; and How and over what time span do initial conditions affect the circulation driven by transient winds?

Statistically significant conclusions are not easily obtained from observations in canyons because of the small number of realizations, the difficulty in placing instruments, and the variability of canyon bathymetry. The third purpose is to show that a model study can compliment observations. For example, vertical velocity is not directly measured and must be estimated on the basis of certain assumptions (say, that horizontal temperature advection is small). It is not easy to justify these assumptions with observations because of the low resolution or short time spans. Models can be used to evaluate some assumptions made in the observational analysis and to help determine if an observed feature is unique to a specific event and bathymetry or is general for similar shapes and forcing.

The above objectives are too grand for a single paper. We have limited the study to conditions (bathymetry, stratification, and forcing) related to Astoria Canyon and to times when winds are mostly upwelling favorable, although a case with downwelling winds is added for contrast. Under these restrictions we will consider the above objectives in two papers. This paper deals with circulation in canyons driven by steady winds, while J. M. Klinck *et al.* (Circulation near submarine canyons: Transient wind forcing, submitted to *Journal of Geophysical Research*, 2000, hereinafter referred to as Klinck *et al.*, submitted manuscript, 2000) considers circulation driven by time variable winds. Our intention is to continue this study to look at how changes in bathymetry, stratification, and forcing modify the results presented here.

Section 2 presents details of the the numerical model, canyon bathymetry, parameter choices, and error analysis. Section 3 presents the model results for three cases. Section 4 analyzes these cases and describes the various processes. Section 5 considers the implications of these results. Section 6 gives conclusions.

2. Methods

2.1. Model Description

We use version 1.0 of the Rutgers University Ocean Model (ROMS), which uses a modified terrain-following coordinate (s coordinate), which can be stretched at the top and bottom to provide higher resolution [Song and Haidvogel, 1994] to better resolve surface and bottom frictional layers.

2.1.1. Domain and canyon bathymetry. The model domain (Figure 1a) is 80 km in the alongshore (x) direction and 80 km in the cross-shore (y) direction. Consistent with a canyon on the west coast of North America, positive x points northward and positive y points westward (offshore). A small region surrounding the canyon (40 km alongshore and 66 km across shore) is used to display the simulation results.

The s coordinate system (Figure 1b) is constructed with parameters θ_s = 5, θ_b = 0.98 and T_{cline} = 200. The first parameter increases the grid resolution above T_{cline}, while the second parameter splits the increased

resolution between the surface and the bottom, with the surface getting slightly preferential treatment.

The domain is periodic in the alongshore (x) direction; the coast is a free-slip wall, while the offshore boundary is open. At the offshore boundary all variables (surface elevation, velocity, and density) are required to have no across shore (y) gradient. No smoothing or additional dissipation is imposed at this boundary.

The bottom topography is constructed from a linearly sloping continental shelf and an outer shelf and slope based on the hyperbolic tangent. The submarine canyon incises both the continental shelf and the offshore slope (Figure 1a). The canyon bottom along the axis depends on the square root of the offshore distance, and the width has a Gaussian shape. The topographic parameters are chosen to be similar to Astoria Canyon [Hickey, 1997] so that the model results can be compared to these observations.

The shelf deepens linearly from 50 m (H_c) at coastal wall to 150 m (H_{sb}) at the shelf break (y_{sb}), which is
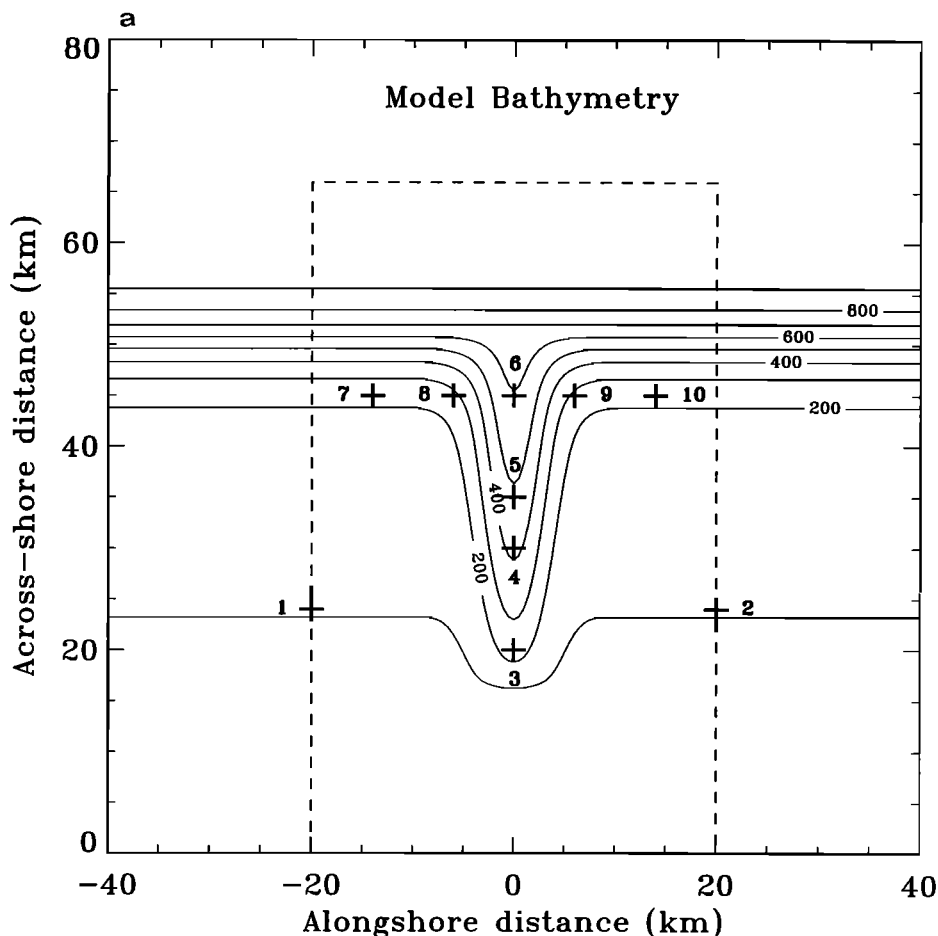

Figure 1. Model Domain, canyon bathymetry, and vertical grid. (a) The solid lines are isobaths with an interval of 100 m. Pluses indicate station locations at which time series of model values are obtained. The dashed line encloses a subregion for which results are displayed. (b) This cross section is along the canyon axis, showing the location of vertical velocity points. Vertical lines are shown at every other grid location. Sloping lines indicate every s coordinate surface.
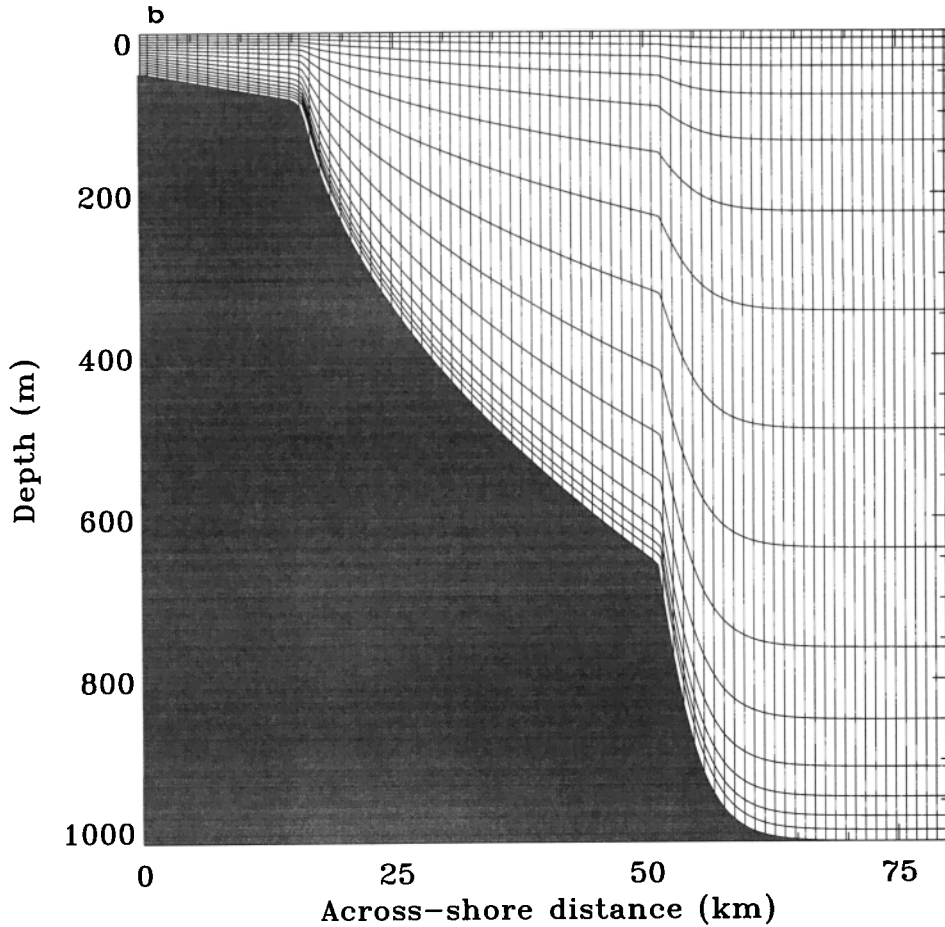
b

Figure 1. (continued)

30 km offshore. The offshore ocean is 1000 m deep (H_{oc}), the approximate water depth at the mouth of Astoria Canyon. A canyon is created with a maximum depth (distance from free surface to bottom at the mouth, d_{can}) of 600 m. Away from the canyon, the continental shelf depth is

$$H_s(y) = H_c - (H_{sb} - H_c)\min(y/y_{sb}, 1)$$
$$+ \frac{H_{oc} - H_{sb}}{2}\left[1 + \tanh(\frac{y - y_{sl}}{L_{sl}})\right],$$

where $y_{sl} = 50$ km is the location of the middle of the slope and $L_{sl}(= 5$ km) is the half-width of the slope.

Coastal canyons tend to be triangular in shape so the width $(W(y))$ for the canyon increases offshore,

$$W(y) = W_c(0.5 + \frac{y}{L_y}),$$

where the canyon width scale (W_c) is 2 km. The depth of the canyon along the axis relative to the surrounding shelf is

$$H_{can}(y) = \max\left(0., -H_s(y) + d_{can}\sqrt{\frac{y - y_c}{y_{sb} - y_c}}\right),$$

where $y_c(= 15$ km) is the location of the head of the canyon. The complete bottom topography is created from these functions as

$$H(x,y) = H_s(y) + H_{can}(y)\exp\left[-\left(\frac{x - x_c}{2W(y)}\right)^2\right],$$

where $x_c(= 0)$ is the location of the axis of the canyon (Figure 1a).

Topographic slopes in Astoria Canyon are as large as 45%, which would cause problems with terrain following vertical coordinates (details below). To reduce the topographic slopes the bottom of the canyon is rounded compared to Astoria. The model canyon is also wider (14 km) than Astoria (10 km). The steepest slope in the model is 8.5%. The model canyon remains narrow since the canyon mouth is about equal to the internal radius of deformation [*Klinck*, 1988] (details below).

The model canyon bathymetry is different from Astoria in other, potentially important, ways. The distance from the coast to the shelf break decreases to the north near Astoria, and the axis of the canyon is not normal to the shelf break; the head of Astoria is a little north of the mouth. These two features cause the northern side of Astoria to look wedge-shaped. For the present study we choose a straight shelf break with the canyon oriented normal to shelf isobaths. We defer to a later study the importance of these variations in the shape of the canyon. However, it is useful to keep in mind the

bathymetric differences between the model and Astoria Canyons as we compare results.

2.1.2. Parameter specifications. Model variables are the three components of flow, density, and surface height. The temperature array in the model is used to hold density, and the specification of a linear equation of state with a thermal expansion coefficient of 1.0 makes the temperature and density equivalent. Salinity is not active in these simulations. The model has a 0.5 km horizontal grid spacing (distance between like variables) and 16 vertical layers. The Coriolis parameter is assumed constant ($f = 1.13 \times 10^{-4}$ s^{-1}). Vertical viscosity and diffusivity are determined by the parameterization presented by Large et al. [1994] which includes effects due to shear instability and density convection. The model allows viscosity and diffusivity to be as small as 10^{-4} and 10^{-5} m^2 s^{-1}, respectively, with largest values of 5×10^{-3} m^2 s^{-1} for both. The critical Richardson number is 0.7. Density inversions produce viscosity and diffusivity of 10^{-2} m^2 s^{-1}. Horizontal Laplacian diffusivity is weak (10 m^2 s^{-1} for velocity and 5 m^2 s^{-1} for temperature). To avoid resolving the surface Ekman layer, the wind stress is applied as a body force over the top three layers (depth ranges from 9 m at the coast to 43 m at the offshore boundary). Bottom friction is parameterized with a quadratic bulk formula with a coefficient of 3×10^{-3}. For all the cases the time step is 2.4 and 60 s for the fast and slow dynamics, respectively.

The initial density field, a functional fit to observations near Astoria [Hickey, 1997], is horizontally homogeneous;

$$\sigma(z, t = 0) = 27.34 - 4.5 \exp\frac{z}{110},$$

where z is the depth in meters. The first internal mode from this stratification has a radius of deformation of 12.7 km. A weaker stratification, with one quarter of this strength, is used in one simulation, producing a radius of deformation of 6.4 km. The canyon is not necessarily narrow for the weaker stratification.

2.2. Model Error Considerations

Two sources of error in the numerical model are of particular concern: steep topography with terrain-following coordinates and periodic continuation in the alongshore direction. Before embarking on the simulation study it is necessary to quantify these errors and their time variation. These issues have been stressed in previous studies [e.g., Haney, 1991; Beckmann and Haidvogel, 1993; Mellor et al., 1994; Klinck, 1996] for different applications.

Generally, all terrain-following models have trouble in the presence of steep bathymetry, mainly because of the error in calculating the horizontal pressure gradient with a discrete numerical scheme [Haney, 1991; Mellor et al., 1994]. ROMS uses some efficient methods to re-duce the error, such as removing a reference density and using a fourth-order difference scheme in the pressure gradient calculation.

We have run the model as described above with initially level isopycnals but without wind forcing. The resulting flow should remain zero, but errors in the pressure gradient calculation produce maximum speeds after 5 days of 0.0074 m s^{-1} at 300 m depth. Maximum error flows at other depths range from 0.0077 to 0.0042 m s^{-1}. The horizontal average of error flows at various depths ranges from 0.0002 to 0.0008 m s^{-1}, which are at most 1.6-2.5% of the wind-driven flows described in this paper. These errors are small enough not to affect these model results. Furthermore, the wind-forced signals are very clear, especially in the transient wind forcing case (Klinck et al. submitted manuscript, 2000), so these small errors do not mask the circulation that we are analyzing.

With periodic alongshore boundary conditions, disturbances that should radiate from the canyon reappear upstream, contaminating the results. These disturbances are due to surface and internal gravity waves, coastal trapped waves, and advection. The surface gravity wave is very fast but is generally small in amplitude. The first-mode internal waves travel at 0.6-1.3 m s^{-1} (for depths of 900 and 150 m, respectively) but also tend to be somewhat small in amplitude. The effects of coastal trapped waves, because of the slow propagation speed, are small in the first 10-15 model days. These vorticity waves travel at 0.2-0.3 m s^{-1}, taking 6-10 days to circle the domain. Furthermore, the alongshore current driven by upwelling winds is opposite to the shelf wave propagation so the contamination is delayed. Simulations show that dynamic instabilities (similar to those described by Barth [1989, 1994]) occur in the model after 3 weeks of steady forcing, so we limit the analysis to the first 15 days of simulation. Finally, ongoing simulations with open boundary conditions (details not given) show that contamination by waves in the periodic environment is, for the most part, small although some important differences do occur in the deeper flow (M. S. Dinniman and J. M. Klinck, manuscript in preparation, 2000).

2.3. Cases

Three cases are described in this paper, representing wind-driven flow over a continental shelf with a submarine canyon. Upwelling winds near Astoria Canyon [Hickey, 1997] have peak speeds near 10 m s^{-1} (stress is about 0.1 N m^{-2}), but typical winds are weaker, with a stress of 0.05 N m^{-2}. The first case uses typical Astoria stratification and is forced by winds (0.05 N m^{-2}). Stronger upwelling winds (0.1 N m^{-2}) drive similar flow with somewhat higher amplitudes (results not shown). The second case is forced by upwelling winds (0.05 N m^{-2}) but with stratification reduced by a factor of 4. Finally, a third case has Astoria stratifi-

cation with moderate (0.05 N m^{-2}) downwelling winds, just to see the difference in behavior. All of these cases were run for 20 days or longer but only the first 15 days of the simulations are described here.

3. Results

The first case, with Astoria stratification and upwelling winds, is used as the standard scenario; the steady features are compared to observations to show close comparison of the numerical results to the observed flow. Simulations are analyzed at three levels (50, 150, and 300 m) representing the water over the shelf, near the canyon rim, and within the canyon, respectively. Vertical sections of density across the shelf display the vertical and horizontal structure. Time histories of flow and integrated transport are used as diagnostics. Results from the other cases are compared to the standard scenario.

Despite the steady forcing the model does not settle into a true steady state. A relatively rapid adjustment occurs in the first 5 days as the upwelling winds

modify the upper water column and establish a conventional upwelling front. However, upwelling within the canyon continues throughout the simulation, so there is slow, continuous change. After about 20 days the frontal flow over the shelf develops meanders that become unstable, creating large eddies. This issue is resolved by the fact that winds over continental shelves are not steady but vary in strength. Simulations with time variable winds, discussed by Klinck et al. (submitted manuscript, 2000), do not develop large-amplitude eddies. Time variability plays another role by clouding, to some extent, the comparison of the steady forced model results with observations that are affected by variable forcing. We will see that the response of the model, and by implication, the continental shelf flow, is rather rapid so both systems are largely in equilibrium with the slowly varying surface forcing.

3.1. Reminder of Astoria Observations

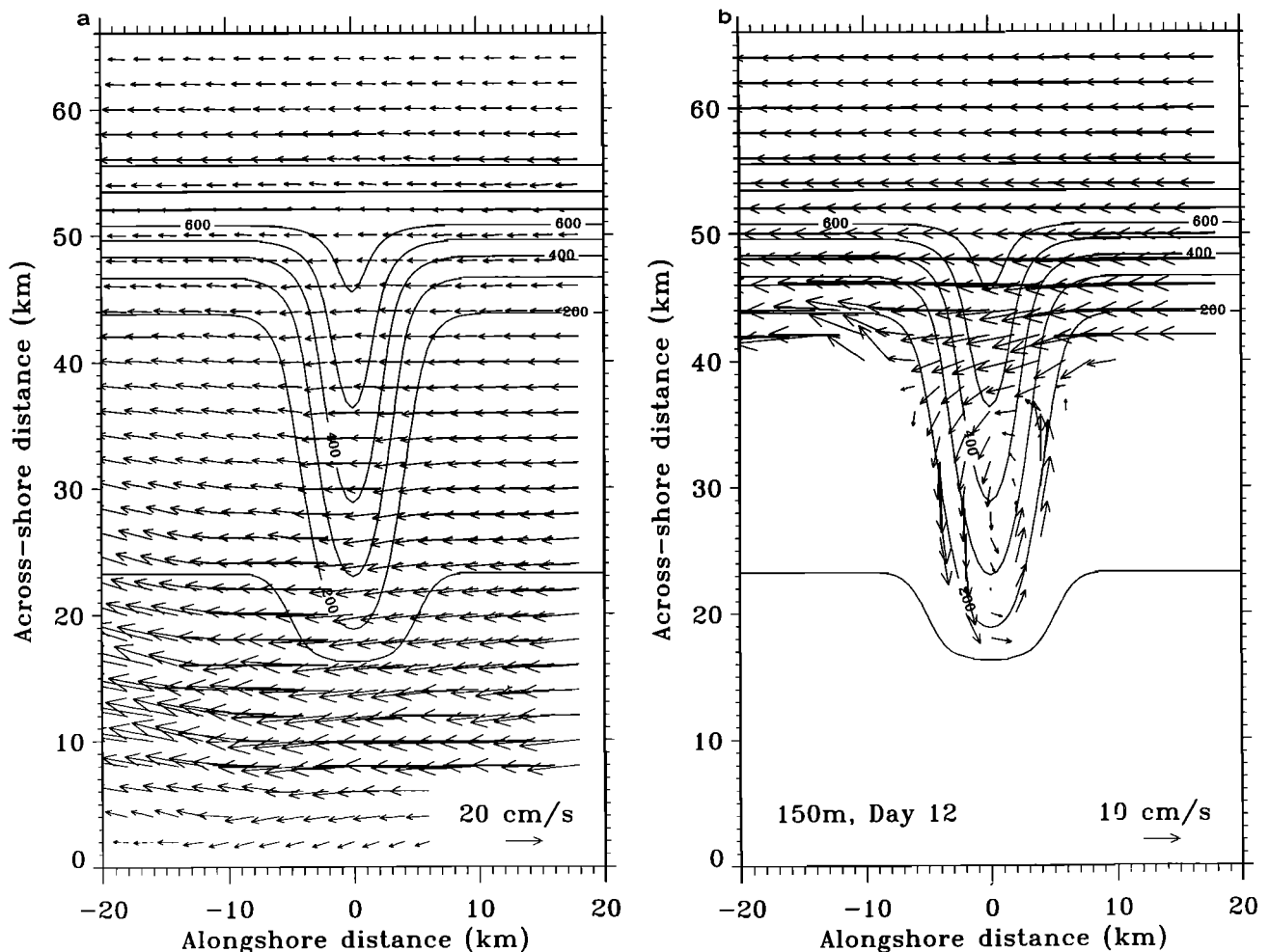Observations reveal three features that need to be represented in any realistic simulation. First, canyon to-

Figure 2. Horizontal velocity vectors at selected depths at model day 12 for upwelling winds over Astoria stratification: (a) at a depth of 50 m, (b) at a depth of 150 m, and (c) at a depth of 300 m. Vectors are shown at every other model grid point, only in the vicinity of the canyon. Solid lines are isobaths with an interval of 100 m.
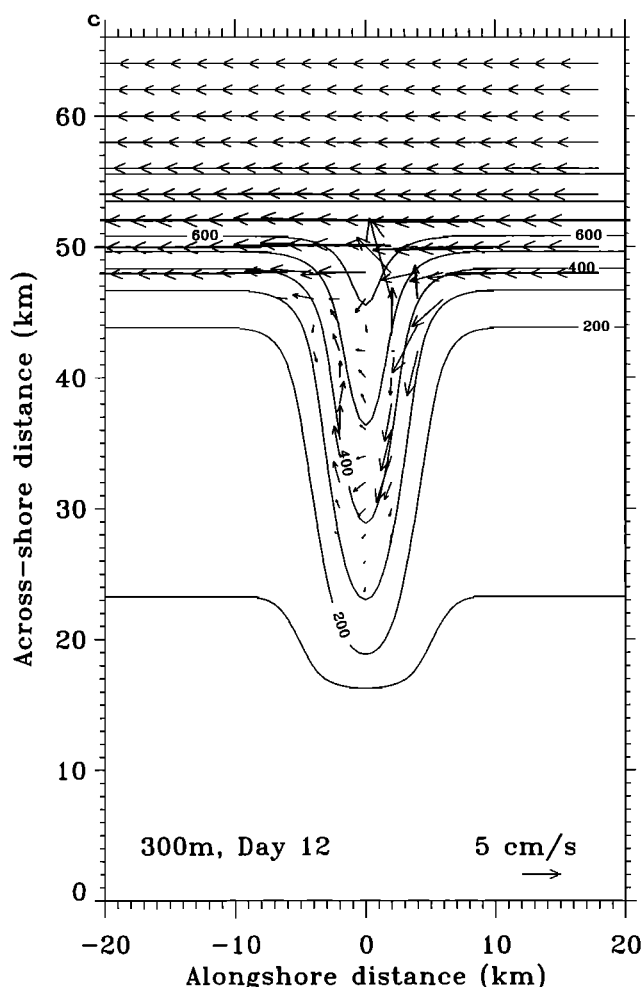
Figure 2. (continued)

pography has little influence on upper layer flow across a canyon [*Hunkins*, 1988; *Hickey*, 1997]. Second, the time mean (over several weeks) circulation within Astoria Canyon driven by upwelling winds is an apparently trapped cyclonic eddy [*Hickey*, 1997]. Third, during times of weak incident flow (i.e., Rossby number < 0.25), cyclonic circulation penetrates vertically a distance 40-100 m above the canyon.

Observations [*Hickey*, 1997] reveal patterns in isotherm depths that can be compared directly with model results. The stratification over the shelf near Astoria Canyon has a strong thermocline at about 100 m. At times of maximum upwelling winds, isotherms near and above the canyon rim tilt upward on the downstream side and downward on the upstream side of the canyon. Below the canyon rim the isotherm tilt is opposite [*Hickey*, 1997, Figure 18]. Distances between isotherms deep in the canyon are larger during upwelling winds.

3.2. Upwelling Winds With Astoria Stratification

3.2.1. Horizontal structures. Model circulation from the first case (upwelling wind forcing with Astoria stratification) is considered at three levels (Figure

2) at model day 12 in the vicinity of the canyon. The fundamentally three-dimensional nature of the flow is evident in the differences in circulation pattern at the different levels. At 50 m the flow (Figure 2a) is southward along the shelf driven by the northerly winds. A strong jet (0.3-0.4 m s^{-1}) occurs between 10 and 20 km offshore, which is associated with the upwelling front. A second, weaker (0.1 m s^{-1}) jet occurs along the upper slope (about 45 km offshore). Away from these jets, the alongshore flow is 0.05-0.1 m s^{-1}. The circulation at this level does not react strongly to the canyon bathymetry; it turns slightly onshore over and upstream of the canyon and turns offshore downstream of the canyon. The free surface (figure not shown) slope is consistent with a geostrophic balance of flow near the surface and does not react to the canyon. The near-surface circulation shows little evidence of upwelling at the head of the canyon.

Just below the canyon rim (150 m), water flows generally alongshore (0.1-0.2 m s^{-1}) except near the canyon (Figure 2b). Onshore flow occurs between the center and the downstream rim of the canyon. Weak onshore flow occurs at the upstream offshore edge of the canyon but most of the flow along the upstream rim is offshore. A strong closed cyclone is evident in the canyon with the center of circulation shifted upstream of the canyon axis.

At 300 m depth the flow (Figure 2c) outside of the canyon is along the slope (0.05 m s^{-1}), with some deflection near the canyon entrance. Within the canyon the flow follows isobaths but does cross isobaths along the downstream side of the canyon. This circulation nearly fills the canyon, extending from the head to very near the mouth. Onshore flow is stronger than offshore, resulting in upwelling.

3.2.2. Vertical sections. The density change from initial conditions along the canyon axis (Figure 3a) after 12 days shows upwelling clearly, with the strongest density increase in the middle and inner shelf where an upwelling front has separated from the coast. Such development is consistent with simulations by *Allen et al.* [1995] among others. A large density change occurs near the bottom over the shelf and into the upper canyon (100-200 m depth). Weaker upwelling occurs over the shelf break upstream of the canyon (Figure 3b), where upwelling is confined to a bottom frictional layer and the vertical excursion of the water is smaller (smaller density change of the upwelled water).

The alongshore structure of the density change (35 km offshore) after 12 days (Figure 3c) reveals an upward motion of all isopycnals, with the largest change around 150 m depth. Dense water appears at both edges of the canyon, with denser water on the upstream (north) side. However, isopycnals are lifted higher on the south side, as shown in the schematic by *Hickey* [1997, Figure 18]. The strong effect of the canyon is seen by comparing the thin layer of increased density upstream of the canyon to that over the canyon.
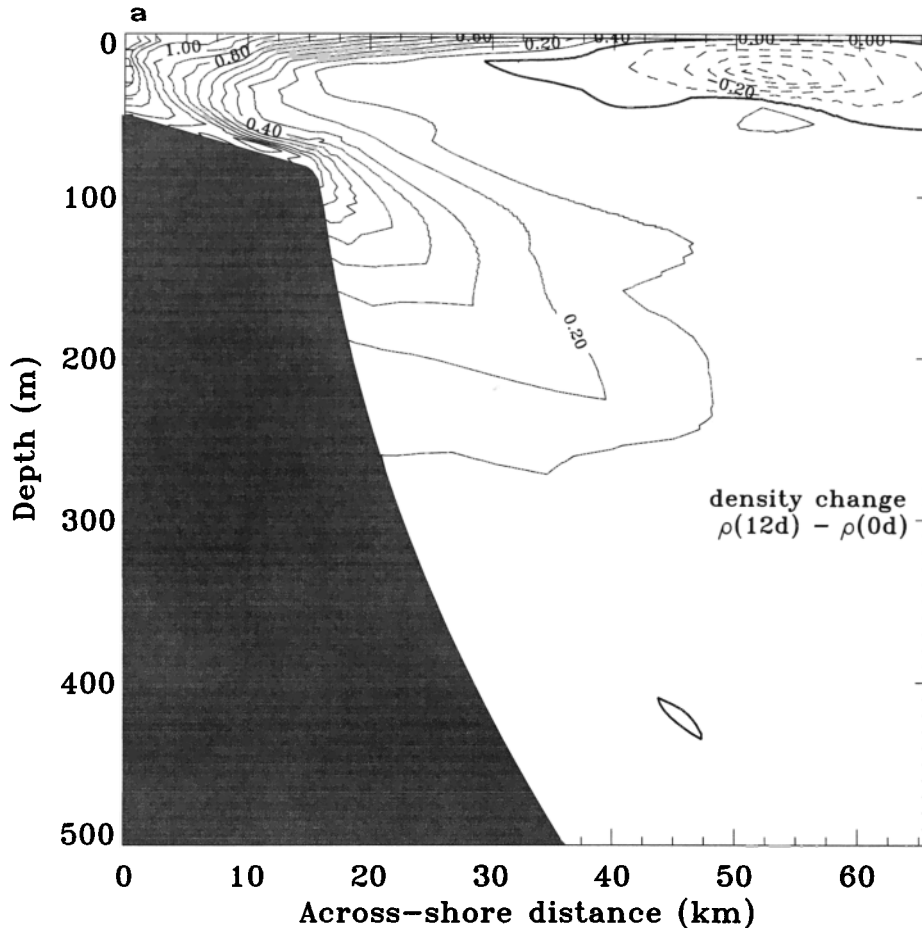
Figure 3. Density change from initial conditions for upwelling winds over Astoria stratification at model day 12: (a) section along canyon axis, (b) section across the shelf 17 km upstream of canyon, and (c) section along the shelf 35 km from the coastal wall. Positive (negative) change is indicated by solid (dashed) contours. The contour interval is 0.1σ. The shading indicates bottom topography. The view is from the coast looking offshore.

The above results are consistent with the mean conditions derived from canyon observations [*Hickey*, 1997] with one exception. The model does not develop a closed cyclonic circulation above the canyon rim, a feature observed over Astoria Canyon when the flow is weak. The Rossby number for this flow is 0.1-0.2, which is in the proper range to develop the cyclone above the canyon.

3.2.3. Time development. The previous analysis assumes that the circulation is steady after about a week, but it continues to change under the influence of steady surface wind stress. Three processes prevent a steady state: wraparound flow due to periodic boundaries, canyon upwelling driven by alongshore flow, and continual offshore migration of the upwelling front, which develops meanders.

Initial circulation in the model undergoes a rapid adjustment to the steady surface forcing, which lasts about a week. After this time the circulation changes at a slower rate until about 3 weeks, when the frontal instability develops. The details of this time develop-

ment are displayed as time and depth plots at a point (Figure 4). Similar behavior occurs at other points.

Alongshore and across shore speed at a point in the center of the canyon about 35 km from the coastal wall (station 5 on Figure 1a) illustrate the time behavior. The alongshore flow (Figure 4a) above the depth of the surrounding shelf (about 150 m) accelerates over about 5 days to speeds of about 0.1 m s^{-1}. There is little vertical shear down to 100 m; the alongshore flow slows significantly in the top 50 m of the canyon, coming to zero at around 175 m. By day 12 the near-surface flow is above 0.15 m s^{-1}, and a clear vertical shear has developed. The velocity shear in the upper canyon has strengthened to the point where the alongshore flow stops over a thickness of about 50 m. The flow at 200 m is opposite to the wind, indicating the development and strengthening of a cyclone (after day 6). Deep within the canyon (below 275 m), water again moves in the direction of the wind, consistent with a deep, anticyclonic swirl.

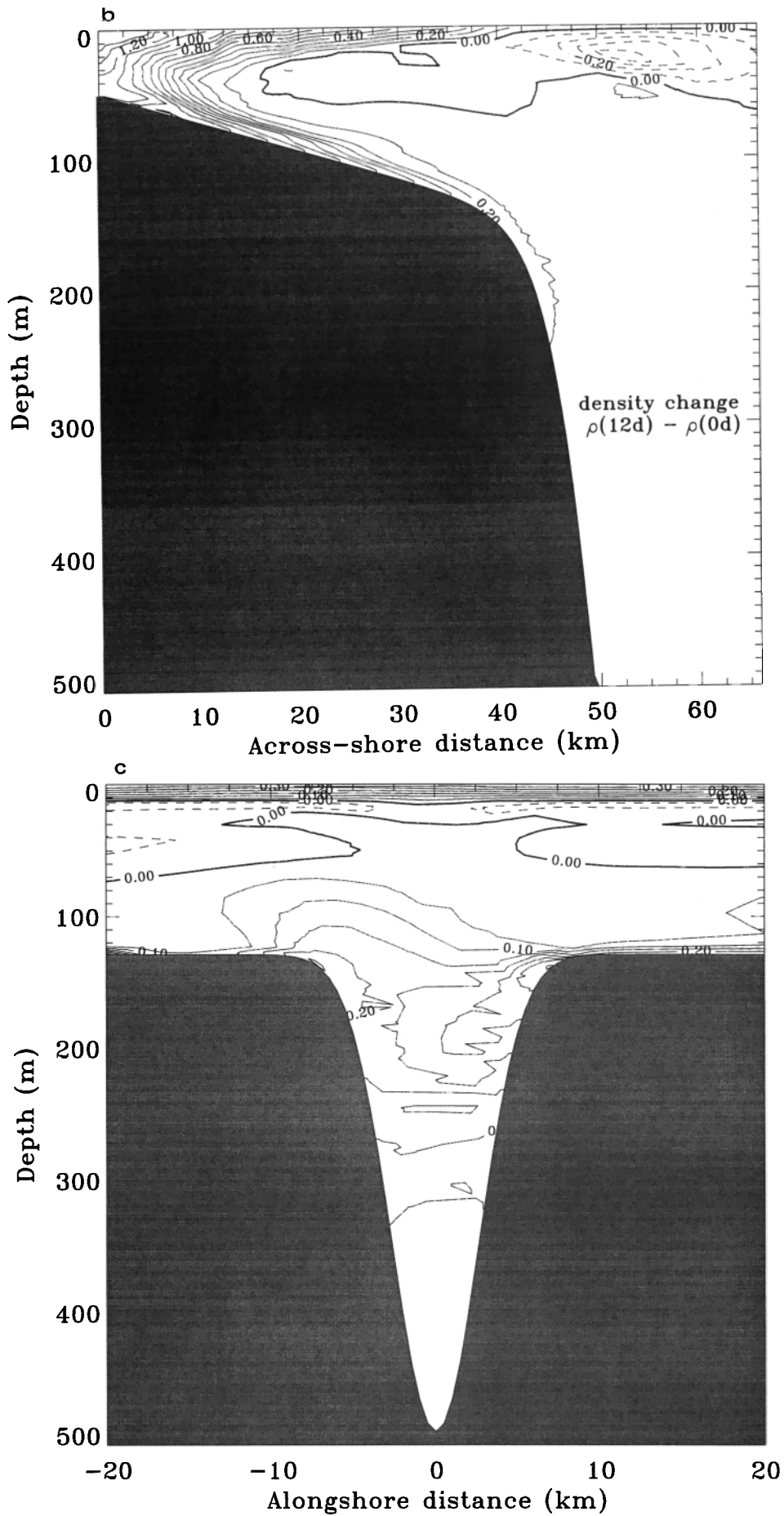The across shore flow at station 5 (Figure 4b) is off-

density change
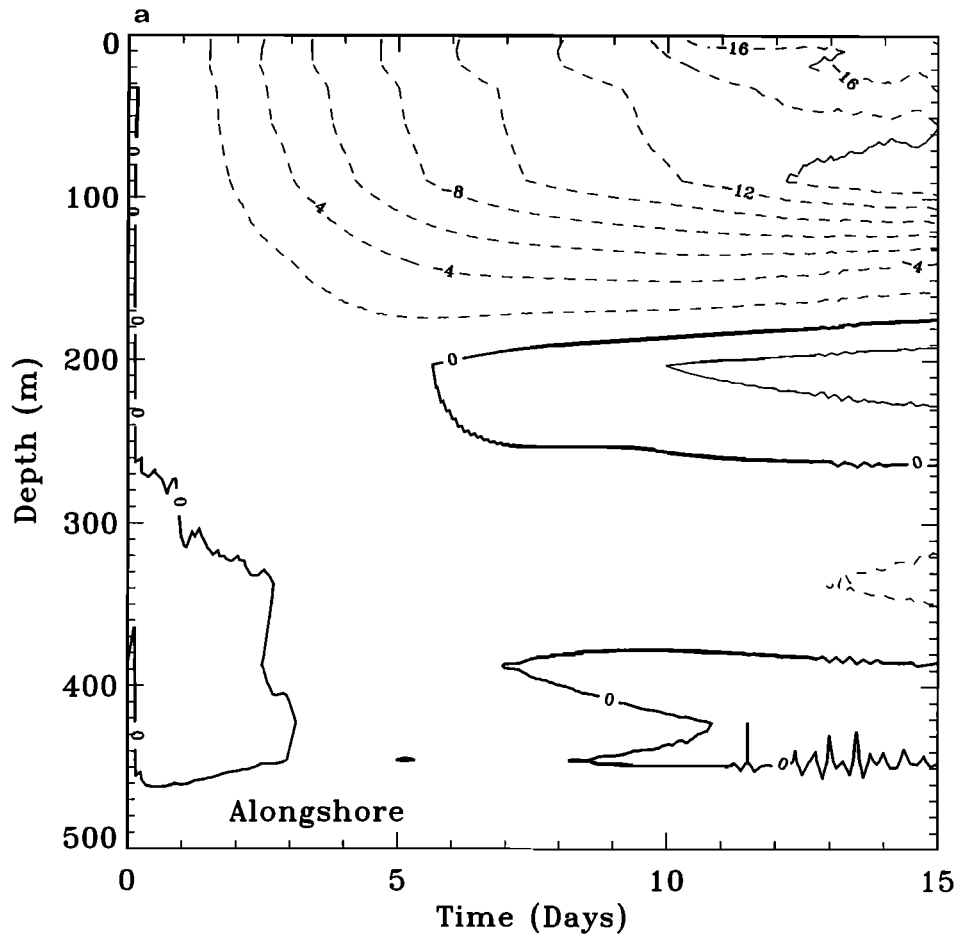$\rho(12d) - \rho(0d)$

Figure 3. (continued)

Figure 4. Vertical and time behavior of flow at station 5 for upwelling winds over Astoria stratification: (a) alongshore speed (cm s^{-1}), with a contour interval of 2 cm s^{-1}, and (b) across-shore speed (cm s^{-1}) with a contour interval of 1 cm s^{-1}. Positive (negative) speed is indicated by solid (dashed) contours.

shore above 30 m throughout the simulation consistent with the offshore Ekman flux. Compensating onshore flow develops down to 300 m, with the strongest onshore speed near the top of the canyon (150 m), which strengthens throughout the simulation. Offshore flow below 250 m increases because of stronger swirl flow with an outgoing branch that widens. In summary, the shelf flow above the canyon changes slowly after the initial startup, but the flow into the canyon continues to strengthen throughout the simulation.

A final description of the circulation is obtained from integrated transport calculated across two planes defined by the top of the canyon (150 m depth) and the extension of the shelf break across the canyon (40 km offshore of the coastal wall), which is referred to here as the mouth of the canyon. Each of these planes is divided into four sections by the axis of the canyon and by either 150 m or by the extension of the shelf break (40 km offshore).

The horizontal transport across the shelf break at the canyon mouth (Figure 5a) is calculated over four subareas (labeled north or south and upper or lower). Above

the shelf break the transport is in opposite directions with onshore flow on the upstream side of the canyon (Nu, dotted line) and offshore flow downstream (Su, solid line). Onshore flow is almost always larger than offshore, indicating net onshore flow. The deep transport across the canyon mouth is more time variable. The upstream transport (Nl, dash-dotted line) is onshore for the first week but slows to zero after day 10. The downstream transport (Sl, dashed line) is small but variable for the first week after which it becomes strongly onshore. This time behavior indicates the initial onshore flow on the north side of the axis and the eventual development of the cyclone, which shifts the onshore flow to the south side of the canyon.

The vertical transport over four subareas (labeled north or south and inner or outer) across the top of the canyon (150 m) quantifies the time behavior of exchanges (Figure 5b). Upwelling occurs over the canyon throughout the simulation with the downstream upwelling (Si, solid line) being larger and increasing continuously, while the upstream upwelling (Ni, dotted line) develops over a week and then reverses to down-
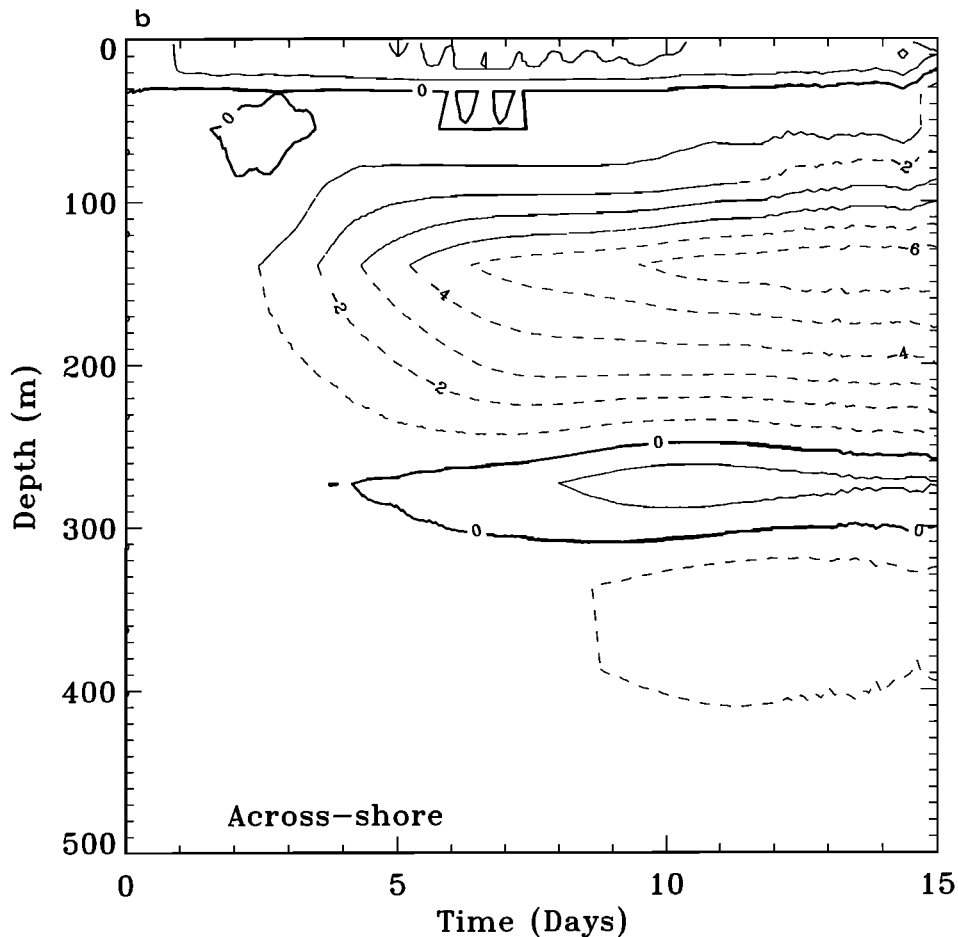
b

Figure 3. (continued)

welling over the remainder of the simulation. The vertical transport offshore of the canyon mouth is affected by the deep topography of the canyon but has opposite signs with upwelling on the upstream side (No, dash-dotted line) and downwelling on the downstream side (So, dashed line) after the initial spin-up. Nevertheless, the upwelling is always larger than the downwelling even offshore of the canyon mouth.

Onshore transport is also calculated at the offshore wall of the model to see the effect of the ocean boundary condition (figures not shown). The transport was calculated over four subareas created by the canyon axis and 150 m. The upper transports are both offshore and constant with magnitudes of 3-4 mSv (1 mSv = 1000 m^3 s^{-1}) until about day 15. The deep transports are both onshore and increase throughout the simulation with values of 5-6 mSv at day 15. Even relatively far offshore, the canyon distorts the alongshore flow, creating a net onshore flow in the deeper layers needed to balance the water that is upwelled through the canyon. It is not that water from far offshore upwells in the canyon but rather that water at depth along the slope is replaced by a general onshore flow, which pulls water through the offshore boundary. Considerable flow

distortion would occur if the offshore boundary were a solid wall.

3.3. Reduced Stratification With Upwelling Winds

The importance of stratification is considered by reducing the initial stratification to one quarter of that from Astoria, thus reducing the internal radius of deformation by half (6.4 km). The simulation is forced by steady upwelling winds (0.05 N m^{-2}).

Bottom topography has a stronger effect on the near-surface flow after 12 days of forcing (Figure 6a) where there is clear onshore turning of the flow upstream of the canyon, onshore flow over the canyon, and an offshore turning downstream of the canyon. Note that even flow in the upwelling jet along the coast turns offshore downstream of the canyon. Just below the canyon rim (Figure 6b) the flow is everywhere into the canyon. Offshore flow develops in the inner canyon along the upstream rim, indicating the development of a cyclone. The deeper flow (Figure 6c) is onshore over most of the canyon with a weak offshore flow along the downstream rim. The flow along the continental slope is largely unaffected by the canyon at these three depths.
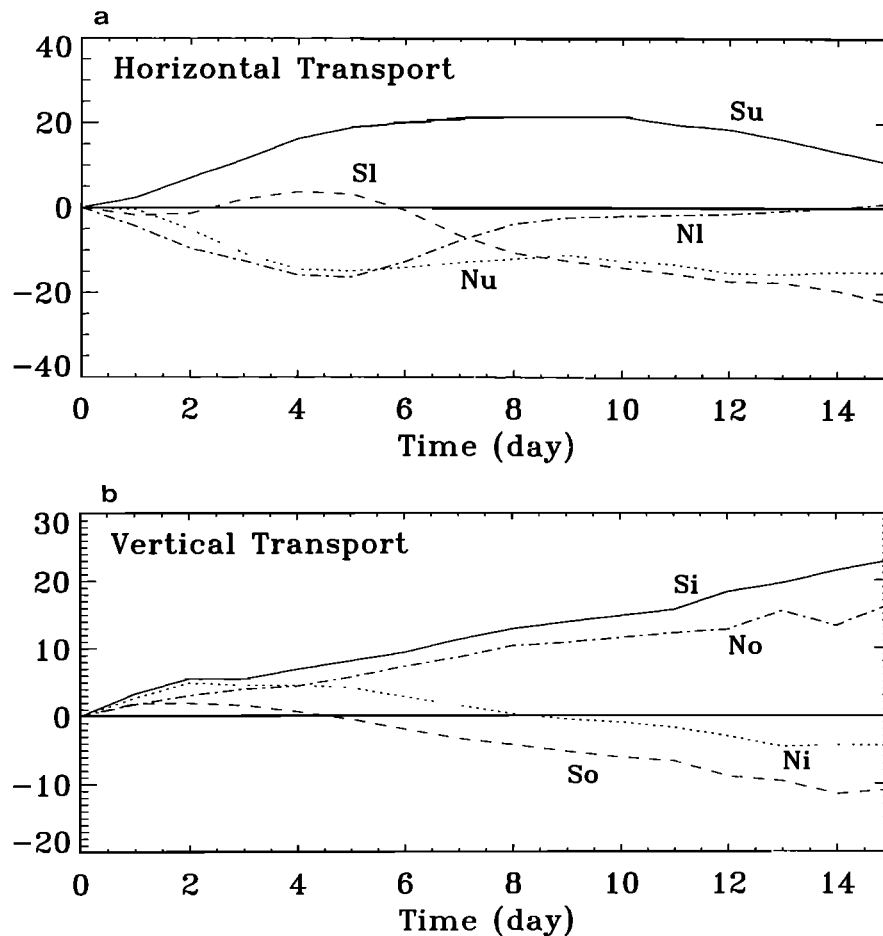
Figure 5. Time series of transport for upwelling winds over Astoria stratification. The units are 1000 m^3 s^{-1}: (a) across shore transport at the canyon mouth (40 km from the coast) over four planes created by 150 m depth and the canyon axis, and (b) vertical transport across the top of the canyon (150 m) over four planes created by the extension of the shelf break and the axis of the canyon. The symbols are N, north; S, south; i, inner; o, outer; u, upper; and l, lower.

Upwelling at the head of the canyon is evident from the density difference at 12 days relative to the initial density (figure not shown), which looks very much like Figure 3a but with reduced values. The depth of maximum density change remains near 200 m. The density change in a section across the canyon looks like Figure 3c with smaller values. The density change contours tilt more strongly in this case, with the 0.1 change contour tilting by 50 m across the width of the canyon with reduced stratification while the 0.2 contour in Figure 3c has very little tilt. The weaker stratification allows a stronger lifting of the isopycnals.

The reduced vertical shear in the horizontal velocity is evident in the time series of flow over depth at station 5 in the head of the canyon (Figure 7). The alongshore speed becomes relatively steady after about 7 days (Figure 7a). There is a very weak reversal after 10 days of forcing. The across shore speed is everywhere onshore, except in the surface Ekman layer (Figure 7b). After 7 days of forcing the flow is relatively steady. The speed and vertical shear are smaller than in the more strongly stratified simulation (Figure 4).

The across shore transports at the mouth of the canyon (Figure 8a) are similar to those obtained for the stronger stratification. The transports adjust rapidly over the first week, with the upper transports reducing somewhat over the next week. The deeper transports continue to change over the span of the simulation, with net onshore flow after 10 days. The strengthening deep onshore flow on the downstream side of the canyon (Sl, dashed line) relative to that along the upstream side (Nl, dash-dotted line) indicates the downstream shift of the up-canyon flow and the development of the canyon cyclone. Finally, there is more onshore than offshore transport at each level, which provides water to upwell through the canyon (Figure 8b).

The vertical transport through the four sections (Figure 8b) at 150 m is similar to that for the stronger stratification. In this case the inner transports become approximately steady after 6 days or so. Furthermore, the upwelling is stronger on the upstream side of the canyon (Ni, dotted line) compared to the downstream side (Si, solid line), which is opposite to that seen in the simulation with stronger stratification. The region
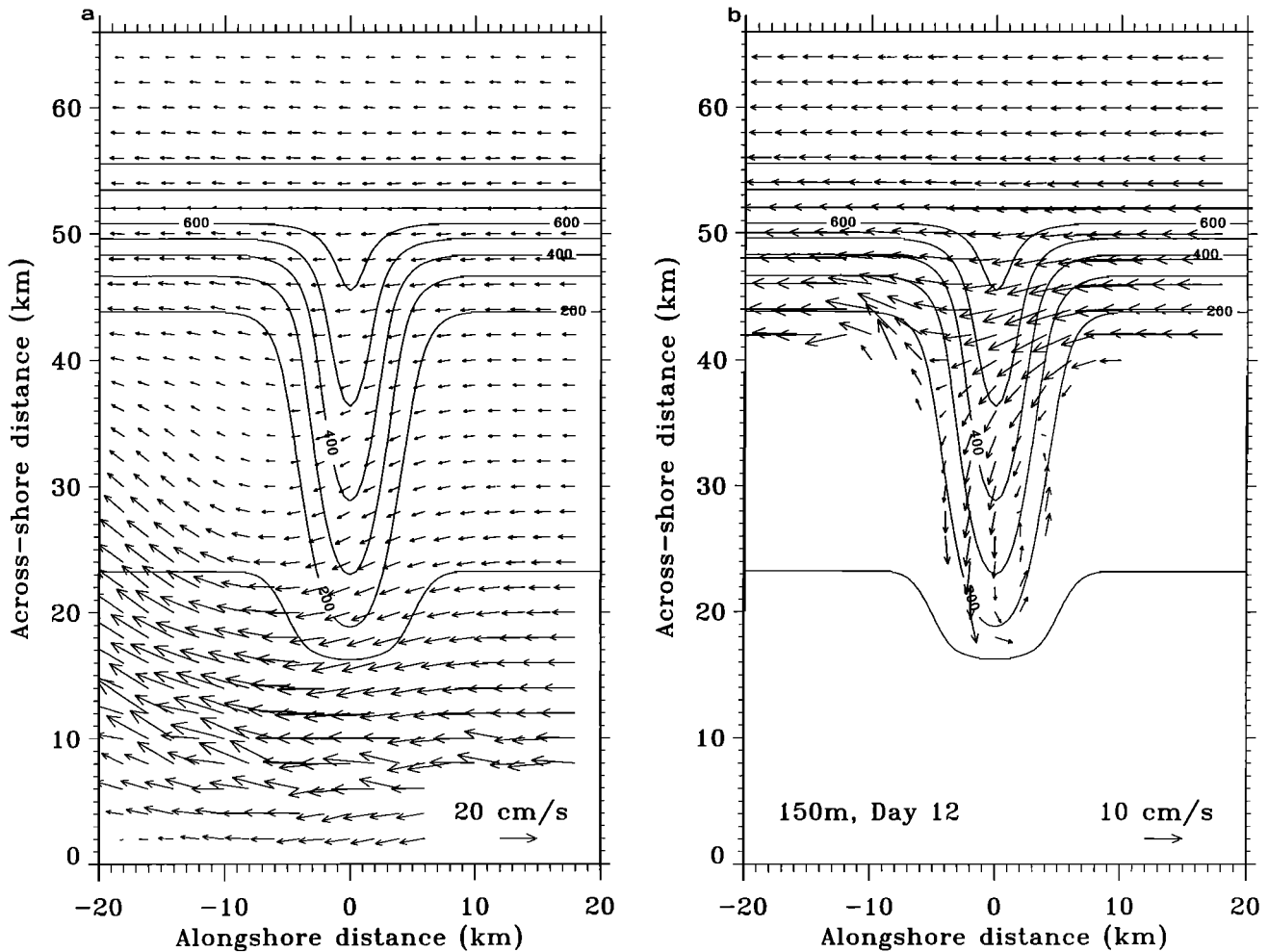
Figure 6. Horizontal velocity vectors at selected depths at model day 12 for upwelling winds over reduced stratification: (a) at a depth of 50 m, (b) at a depth of 150 m, and (c) at a depth of 300 m. Vectors are shown at every other model grid point, only in the vicinity of the canyon. Solid lines are isobaths with an interval of 100 m.

offshore of the shelf break is also affected by the canyon topography, with upwelling north of the canyon axis and downwelling south of the canyon. The offshore transport magnitudes are about the same size, indicating little net vertical motion.

3.4. Astoria Stratification With Downwelling Winds

If the dynamics were linear, then reversing the direction of wind would merely change the sign of all of the upwelling results. These expectations are largely true above the shelf depth, although nonlinearity does play a role in the upper layers. Deeper flows differ substantially with reversal of winds.

The downwelling forced flow over the shelf (figure not shown) is the opposite of that from upwelling winds (Figure 2a). The flow at the depth of the canyon rim (Figure 9a) is northward along the slope and strongly across isobaths along the downstream canyon rim. An anticyclone occurs over most of the canyon. At deeper depths (Figure 9b), water swirls cyclonically through

the canyon following isobaths, although there is more small-scale structure than in previous cases.

The time behavior of alongshore speed at station 5 (Figure 10a) gives the best indication that the flow is just the reverse of the upwelling case (Figure 4a). However, it is weaker than the upwelling case.

The across shore flow (Figure 10b) above 30 m is in the direction of the Ekman flux, but it continues to strengthen over the 2 weeks of forcing. Weak, but generally offshore, flow develops within a 20 m thick layer just below the Ekman layer. In the top of the canyon is a 100 m thick layer, which flows weakly offshore for the first 5 days, followed by relatively strong onshore flow, which by the end of the simulation, turns offshore again. This contrasts to the continually increasing flow with upwelling winds (Figure 4b).

The across shore transport at the canyon mouth (Figure 11a) is rather different from the other two cases. Above the shelf break, there is onshore flow south of the canyon axis (Su, solid line) and offshore flow (Nu, dotted line) north of it, which is the signature of north-
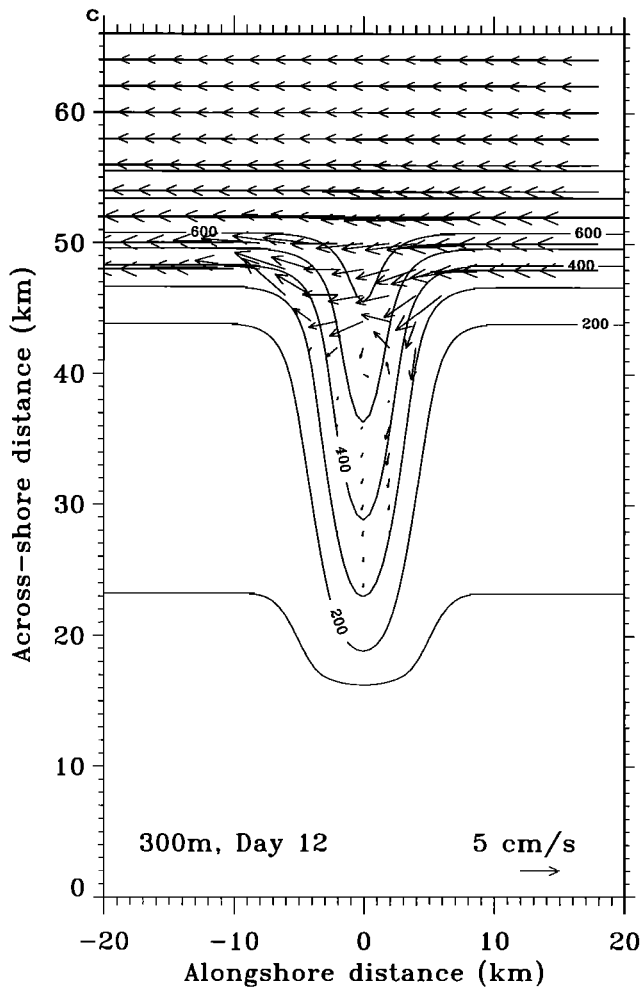
Figure 6. (continued)

4. Discussion

4.1. Circulation Forced by Upwelling Winds

The three-dimensional canyon circulation driven by constant upwelling favorable wind forcing has the following general structure. Above 100 m, there is only small influence of canyon topography with onshore flow over and upstream of the canyon (Figure 2a) and offshore downstream of the canyon. An upwelling front develops near the coast and is closer to the coast upstream of the canyon and more offshore downstream as the shelf flow turns offshore (anticyclonic) downstream of the canyon. Near the canyon rim (100-200 m), flow is onshore (Figure 2b) within the canyon, particularly along the downstream (southern) rim. The deep flow largely follows isobaths (Figure 2c) with some transport imbalance that produces upwelling that extends to 300 m depth.

These results are consistent with previous observations, except for the closed cyclone above the canyon. We can deduce mechanisms driving canyon circulation from these simulations in response to several questions. How does the wind drive up-canyon flow and ultimately upwelling of water onto the shelf? What is the cause of the cyclonic circulation trapped within the canyon? What is the role of momentum advection in canyon circulation? What are the timescales over which these patterns of circulation develop?

4.1.1. Dynamics of canyon circulation.
The answer to the first question lies in the traditional explanation of up-canyon flow, where the key point is the across shore pressure gradient and the narrow steep canyon topography, which inhibits alongshore flow. The canyon topography breaks the geostrophic constraint, allowing across shore flow. Upwelling wind stress creates a geostrophically balanced alongshore flow, which is supported by an onshore pressure gradient over the entire coastal domain. During the first week this pressure gradient drives water into the canyon, creating upwelling. At the head of the canyon, water in all layers is lifted; some water is lifted out of the canyon and deposited on the shelf. There is flow across isobaths along whole rim of the canyon and not just at the head (Figure 2b). Deep upwelling exists within the canyon on the upstream edge (Figure 2c), even though this water never reaches the shelf.

Over time, upwelling tilts the isopycnals largely compensating the surface pressure gradient (Figure 12a) over the top of the canyon. There remains an unbalanced onshore pressure gradient force over the inner canyon except at the head (Figure 12b), which continually drives water into the canyon (Figure 2b). A positive residual offshore force develops along the outer canyon to oppose flow into the canyon and to drive water offshore.

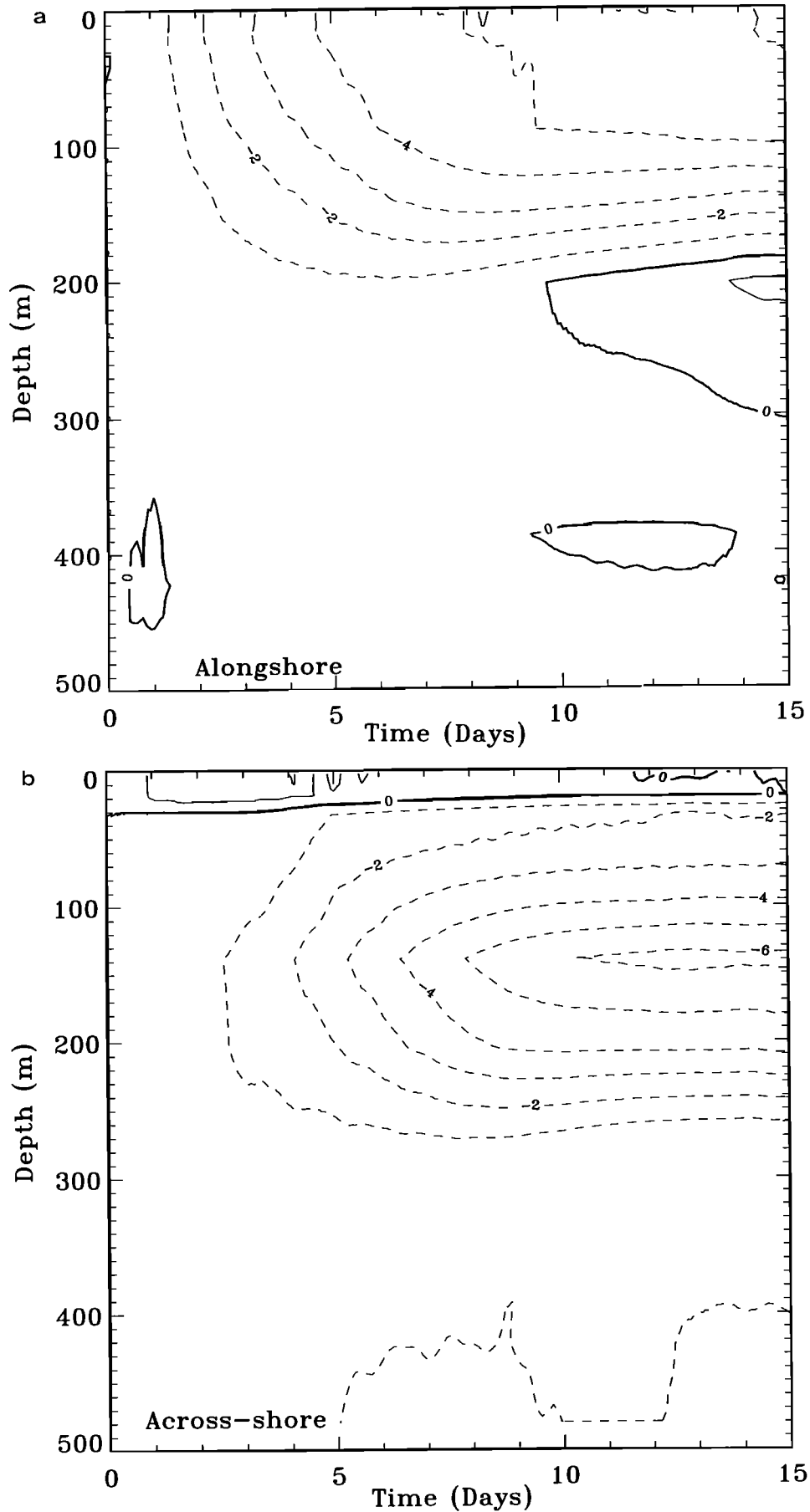Model results indicate that wind-forced coastal up-

ward flow across the mouth of the canyon that dips into the canyon mouth. The onshore transport (Su) is larger than the offshore (Nu) as required for net downwelling over the canyon.

The deep transports (Figure 11a) are largely opposite, with a direction change around 7 days. There is a net offshore deep transport in the first few days, as the downwelling winds depress the isopycnals in the canyon. Around 7 days, the transports switch sign with the development of an anticyclone in the canyon. The strength of the deep transports decline over the second week of the simulation.

The vertical transport through the four areas at the top of the canyon (Figure 11b) is downward over the canyon (Ni, dotted line, and Si, solid line) as well as offshore of the canyon on the north side (No, dash-dotted line). Upwelling occurs offshore south of the canyon axis (So, dashed line). Offshore, upwelling on one side of the canyon axis is stronger than downwelling on the other side. Downwelling occurs over the whole canyon and is stronger over the upstream rim (Si compared to Ni).

Figure 7. Vertical and time behavior of flow at station 5 for upwelling winds over reduced stratification: (a) alongshore speed (cm s^{-1}), with a contour interval of 1 cm s^{-1}, and (b) across shore speed (cm s^{-1}), with a contour interval of 1 cm s^{-1}. Positive (negative) speed is indicated by solid (dashed) contours.
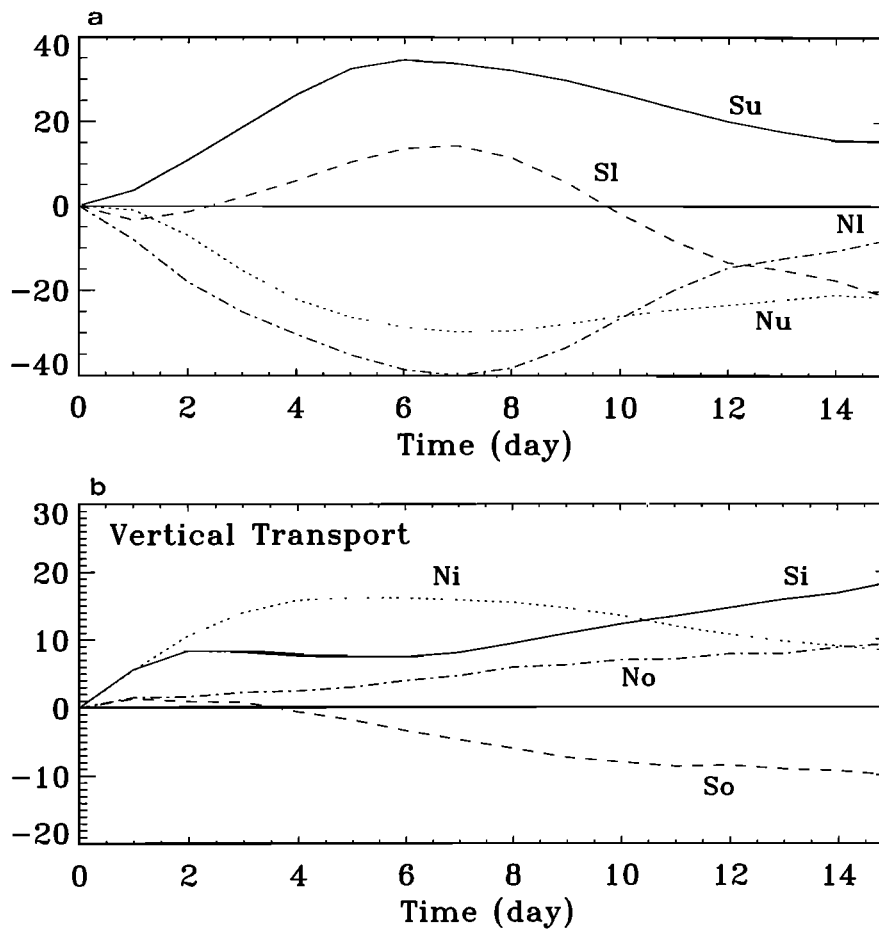
Figure 8. Time series of transport for upwelling winds over reduced stratification. The units are 1000 m^3 s^{-1}: (a) across shore transport at the canyon mouth (40 km from the coast) over four planes created by 150 m depth and the canyon axis, and (b) vertical transport across the top of the canyon (150 m) over four planes created by the extension of the shelf break and the axis of the canyon. The symbols are N, north; S, south; i, inner; o, outer; u, upper; and l, lower.

welling is much weaker away from the canyon than over it. The former produces density changes at the shelf break of 0.1σ (Figure 3b), while the latter produces changes at the head of the canyon about 0.5σ that extend over a greater thickness of water (Figure 3a). The enhanced vertical motion within the canyon is due to onshore flow, which is due to the narrow canyon.

4.1.2. Cause of the canyon cyclone. There are two sources of cyclonic vorticity in the canyon, which play a role in the development of the cyclone (Figure 2b). First is the cyclonic turning of the flow into the canyon, the strength and location of which depends on the flow speed and the details of the bathymetry at the canyon entrance. The circulation considered here is sufficiently strong for momentum advection to cause separation at the upstream corner, pushing the onshore flow closer to the downstream rim. The second source is stretching of planetary vorticity by the vertical motion within the canyon. The water below the maximum density change (Figure 3a) is the region of stretching, while vortex compression occurs above the maximum.

The cyclonic vorticity in the model is comparable to that observed [*Hickey*, 1997]. The swirl speed in the cyclone (Figure 2b) is about 0.1 m s^{-1}, which compares with measurements by *Hickey* [1997, Figure 9a]. The estimated relative vorticity is about 0.4*f* (0.1 m s^{-1} swirl with a diameter of 5 km), which is about half of the value calculated by *Hickey* [1997, Figure 12]. Processes not included in these simulations could further strengthen the cyclone. Flow rectification [*Holloway*, 1987] due to random eddies interacting with topography was proposed as the cause of a trapped cyclone in regions with weak wind forcing [*Hunkins*, 1988]. Phase shift between transient wind forcing and flow generates stronger cyclones (Klinck et al., submitted manuscript, 2000).

4.2. Influence of Stratification

Stratification allows vertical gradients in the flow, reducing the influence of bathymetry. As stratification is reduced to zero (and assuming weak friction), the flow is strongly constrained to follow bathymetric contours. As
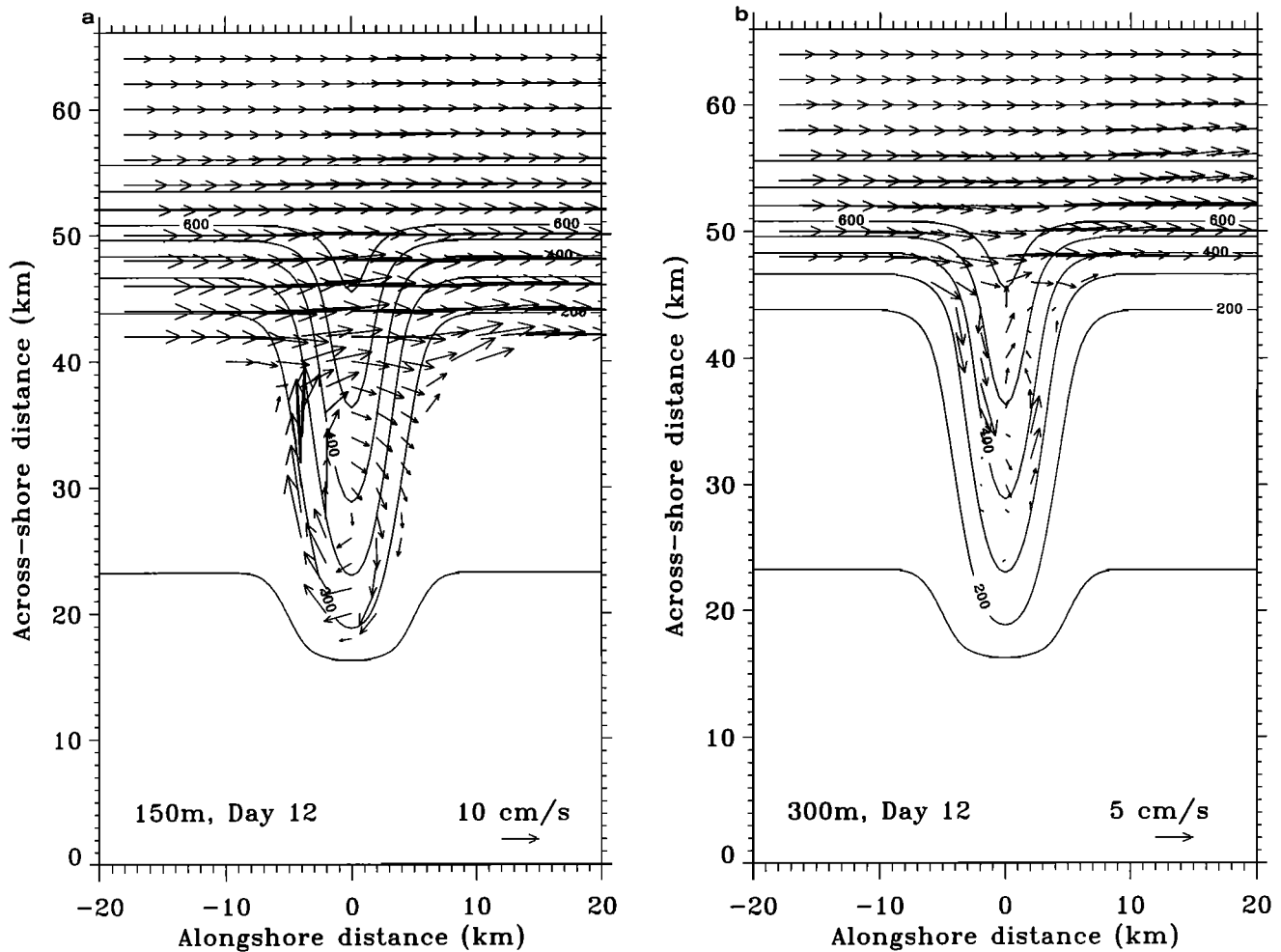
Figure 9. Horizontal velocity vectors at selected depths at model day 12 for downwelling winds over Astoria stratification: (a) at a depth of 150 m, and (b) at a depth of 300 m. Vectors are shown at every other model grid point, only in the vicinity of the canyon. Solid lines are isobaths with an interval of 100 m.

stratification is made very strong, then slight changes in the density structure due to initial upwelling isolates the circulation from the bathymetry.

In the cases considered here, weaker stratification allows more influence of the bathymetry (Figure 6a) on the near-surface flow, weaker onshore flow in the upper canyon but covering more of the width (Figure 6b), and weaker deep flow within the canyon (Figure 6c). Interestingly, the weak stratification case has larger cross-shore transports below 150 m (Figures 5 and 8), but they tend to compensate so that the net onshore transport is smaller. The across shore pressure gradient (Figure 13a) is comparable to that with stronger stratification (Figure 12a), which is not surprising since it is due to the free surface tilt created by the wind. The residual pressure gradient (Figure 13b) is consistently onshore, indicating the inability of the weaker density structure to isolate the canyon from the pressure gradient due to the surface slope.

An additional simulation was run with stratification 4 times that of Astoria driven by constant upwelling winds. In spite of the further doubling of the radius of deformation the resulting flow is not markedly different from the first case. The structure of the flow looks rather like Figure 2 with flow speeds about the same. The depth of upwelling in the canyon was around 300 m. There was reversal of the flow in the deeper sections of the canyon with the development of a deep anticyclone (flow follows isobaths). Such a deep flow was less evident with the Astoria stratification. There is no further qualitative difference in the flow with such increases in the stratification of values stronger than observed near Astoria Canyon.

4.3. Circulation Forced by Downwelling Winds

Circulation forced by downwelling winds is largely opposite to that forced by upwelling winds. A strong anticyclone in the canyon (Figure 9), which is comparable to
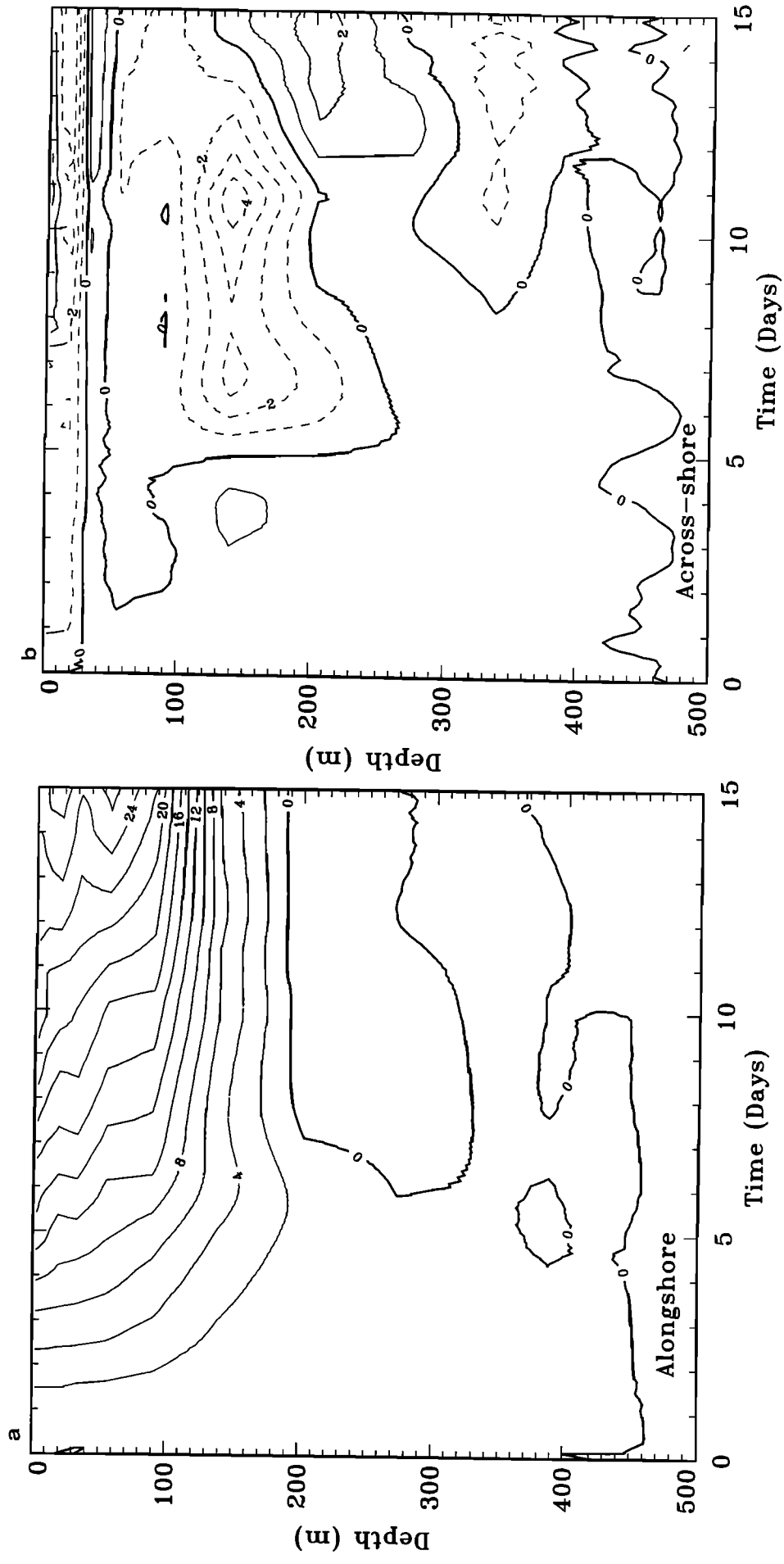
Figure 10. Vertical and time behavior of flow at station 5 for downwelling winds over Astoria stratification: (a) alongshore speed (cm s^{-1}), with a contour interval of 2 cm s^{-1}, and (b) across-shore speed (cm s^{-1}), with a contour interval of 1 cm s^{-1} Positive (negative) speed is indicated by solid (dashed) contours.
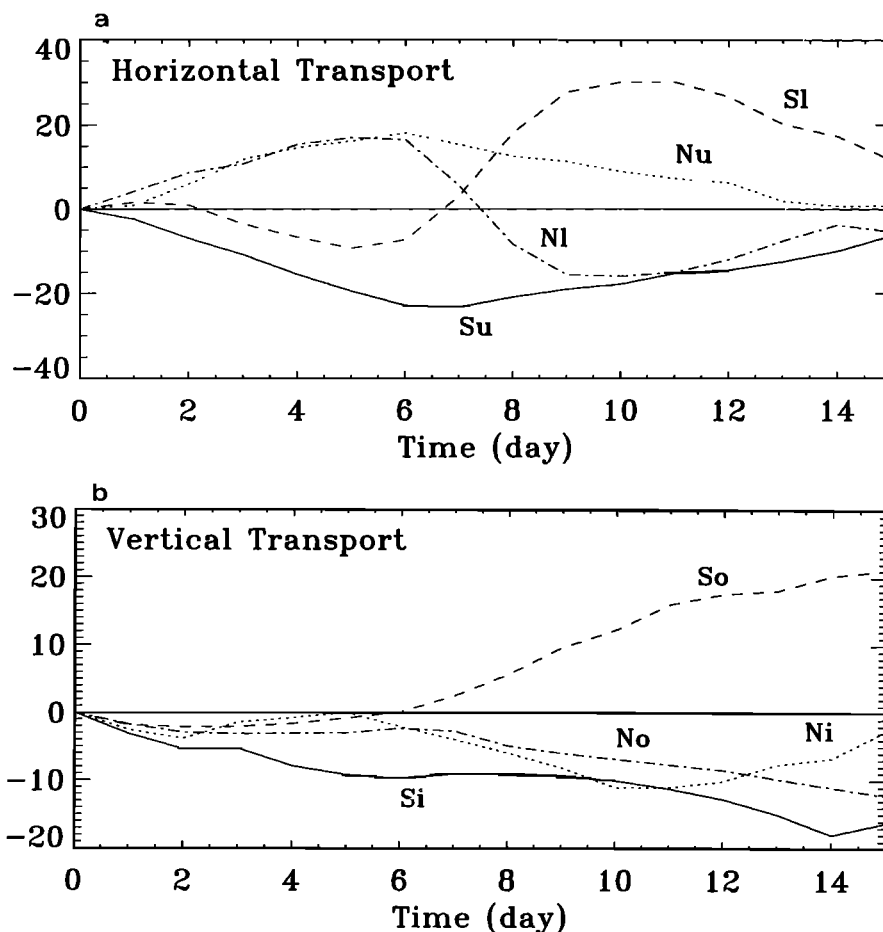
Figure 11. Time series of transport for downwelling winds over Astoria stratification. The units are 1000 m^3 s^{-1}: (a) across shore transport at the canyon mouth (40 km from the coast) over four planes created by 150 m depth and the canyon axis, and (b) vertical transport across the top of the canyon (150 m) over four planes created by the extension of the shelf break and the axis of the canyon. The symbols are N, north; S, south; i, inner; o, outer; u, upper; and l, lower.

the cyclone generated in the upwelling case (Figure 2), is driven by vortex compression or frictional coupling to the alongshore flow. The flow at 150 m (Figure 9a) is directly into shallower water, creating strong flow toward the shelf (causing downwelling, not upwelling). In the upwelling case the cyclone tends to fill the canyon.

Previous numerical results [*Klinck*, 1996] show that right bounded (downwelling) circulation past a canyon causes little net cross-shelf exchange, while left bounded flow produces significant exchange. Wind-driven simulations discussed here differ from previous results by showing a net exchange for either direction of wind forcing. However, upwelling winds produce stronger exchange than downwelling, as seen in the vertical transport time series (Figure 5b and 11b). Also, note that changing the sign of the wind forcing changes the sign of the vertical transport for the first 5 days; that is, the response is largely linear over that time. Beyond that time the transport time series are no longer opposite because of differently developing density structure and nonlinear effects.

The across shore pressure gradient is almost opposite of upwelling with offshore force throughout (Figure 14a). However, it remains nonzero over the canyon, while the upwelling case has a sign reversal; the downwelling case cannot develop sufficient density contrast to compensate the surface gradient. It is interesting that circulation near the top of the canyon with downwelling winds is more alongshore (except at the upstream rim), while upwelling winds create mainly across shore flow. The residual pressure gradient (Figure 14b) has alongshore antisymmetry with onshore residual force upstream and offshore downstream. The residual force in the upwelling case is across shore antisymmetric with onshore force near the canyon head and offshore over the outer canyon.

We note in passing that a thick bottom boundary layer (figure not shown) develops, which also plays a role in decoupling the alongshore flow on the shelf from the bottom topography. This difference between upwelling and downwelling winds also occurs in these simulations, but these features are discussed elsewhere [*Chapman*
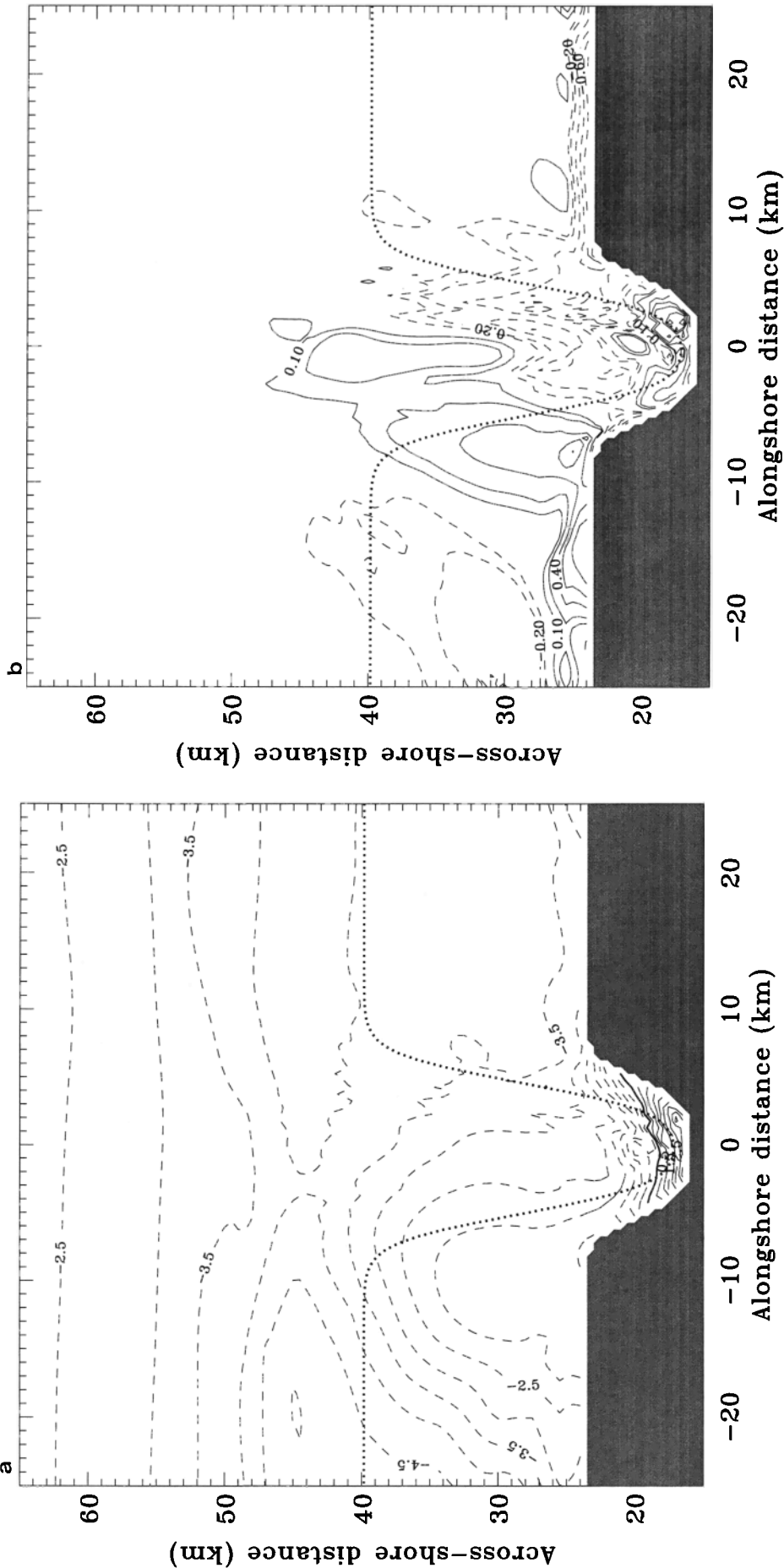
Figure 12. Pressure gradient and ageostrophic forces in the across shore direction for upwelling winds over Astoria stratification at day 12 at 100 m. Each term is integrated over a grid cell; the units are m³ s⁻². Positive (negative) values are indicated by solid (dashed) contours. Shading shows the part of the domain that is below the bottom. The dotted line is the 150 m isobath. (a) Pressure gradient force integrated over a model cell. A positive force accelerates the flow in the positive direction. The contour interval is 0.5 m³ s⁻². (b) Sum of the pressure gradient force and the Coriolis force, which indicates the unbalanced pressure force in the across shore direction. The contour interval is 0.1 m³ s⁻².
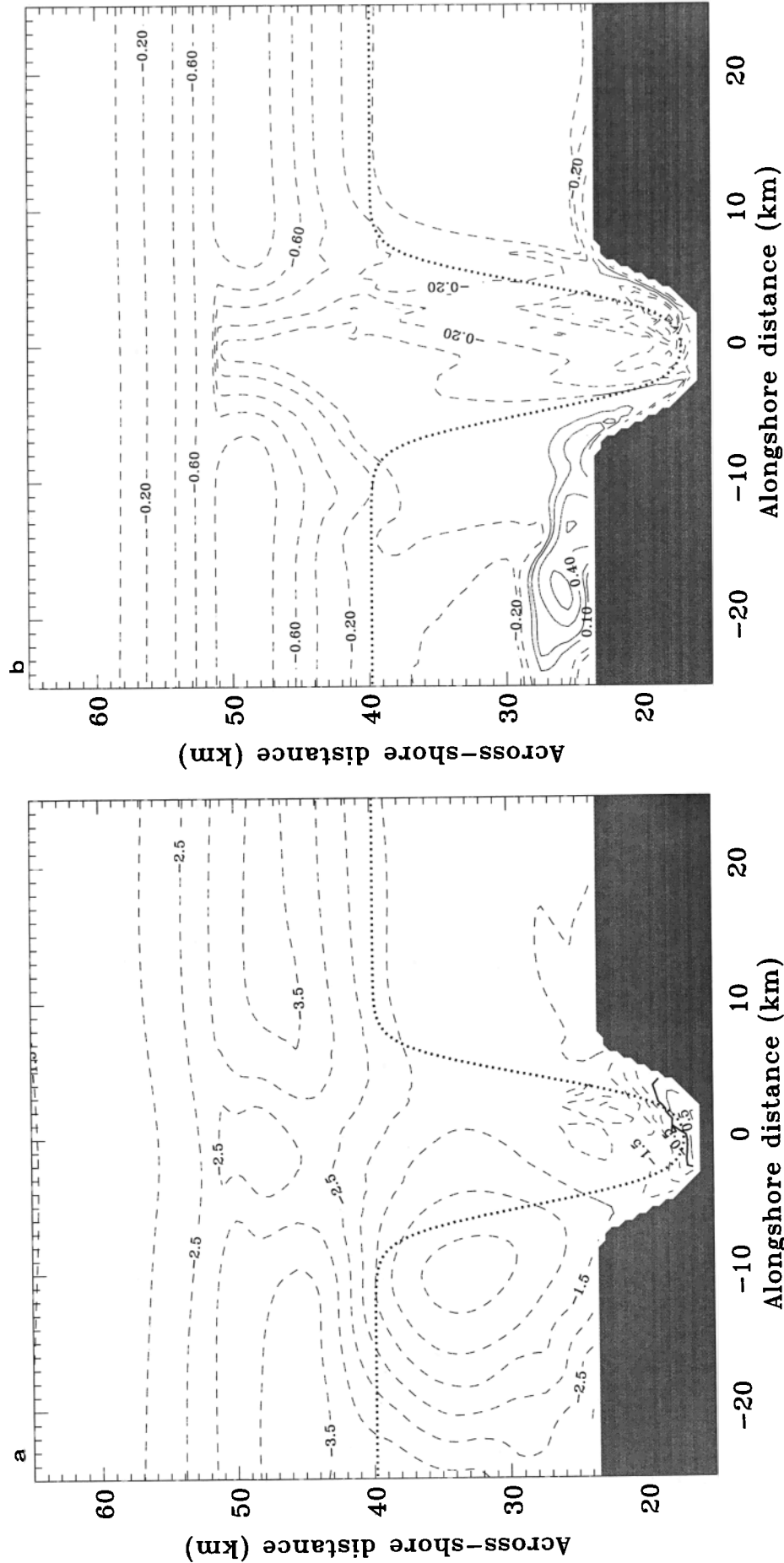
Figure 13. Pressure gradient and ageostrophic forces in the across shore direction for upwelling winds over one quarter Astoria stratification at day 12 at 100 m. Each term is integrated over a grid cell; the units are m³ s⁻². Positive (negative) values are indicated by solid (dashed) contours. Shading shows the part of the domain that is below the bottom. The dotted line is the 150 m isobath. (a) Pressure gradient force integrated over a model cell. A positive force will accelerate the flow in the positive direction. The contour interval is 0.5 m³ s⁻². (b) Sum of the pressure gradient force and the Coriolis force, which indicates the unbalanced pressure force in the across shore direction. The contour interval is 0.1 m³ s⁻².
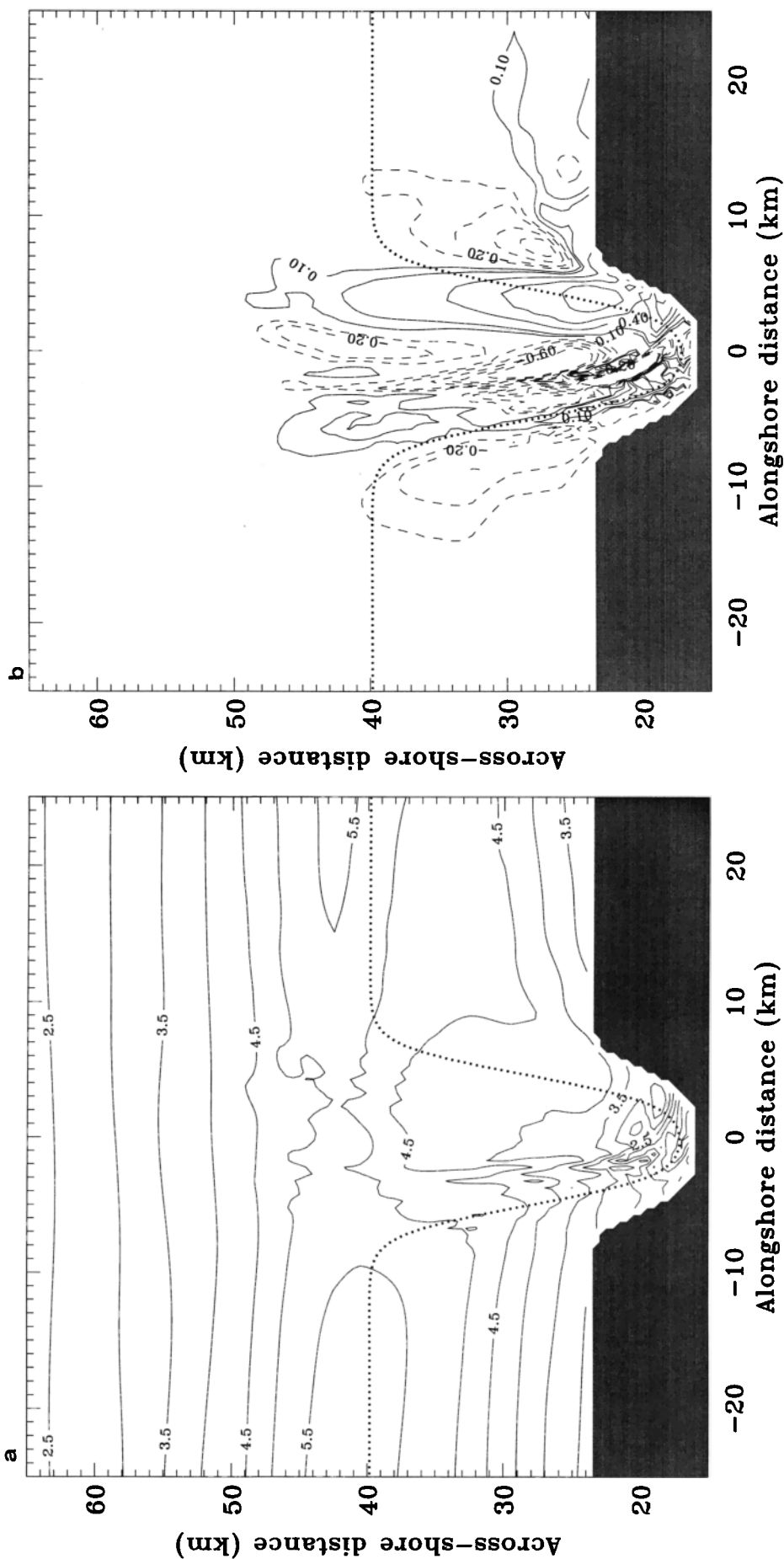
Figure 14. Pressure gradient and ageostrophic forces in the across shore direction for down-welling winds over Astoria stratification at day 12 at 100 m. Each term is integrated over a grid cell; the units are $m^3 \ s^{-2}$. Positive (negative) values are indicated by solid (dashed) contours. Shading shows the part of the domain that is below the bottom. The dotted line is the 150 m isobath. (a) Pressure gradient force integrated over a model cell. A positive force will accelerate the flow in the positive direction. The contour interval is 0.5 $m^3 \ s^{-2}$. (b) Sum of the pressure gradient force and the Coriolis force, which indicates the unbalanced pressure force in the across shore direction. The contour interval is 0.1 $m^3 \ s^{-2}$.

and Lentz, 1997; *Middleton and Cirano*, 1999], and these processes are not dominant in these simulations.

4.4. Influence of Momentum Advection

Momentum advection is important in creating the observed flow patterns near canyons. Upwelling winds drive upwelling within the canyon even without momentum advection (figure not shown). However, the onshore flow is constrained to the upstream edge of the canyon unless advection pushes this flow toward the downstream rim. Thus up-canyon flow, though driven by the surface pressure gradient, requires momentum advection to expand over the canyon. Also, shelf flow is pushed close to the coastal wall (Figure 2a) by onshore flow upstream of the canyon. Without momentum advection the flow along the shelf is largely symmetric (figure not shown), with the water returning to its original distance from the coast after a quick trip around the canyon.

Momentum advection is found to be essential in forming the surface flow across the canyon and the trapped cyclone within the canyon. Without the momentum advection the near-surface flow follows the canyon bathymetry, and the cyclonic vorticity occurs only below 400 m depth (figure not shown).

4.5. Timescale of Response to Winds

We need to know how rapidly circulation near a canyon responds to a change in the wind stress. The timescale allows an estimate of the amount of the dense water transported to the continental shelf by submarine canyons. For Astoria stratification the circulation near the head of the canyon (Figure 4) becomes approximately steady after 5-6 days. The vertical velocity is nonzero as long as the winds blow, so onshore transport continues. Over many weeks it is possible for slow adjustments to modify these results, but we have not investigated such slow changes. Winds over the western North America shelf rarely persist longer than a week [*Hickey*, 1998]; it does not make much sense to ask about the ultimate steady state. Additionally, the periodic model domain produces unrealistic circulation after about 20 days so this model setup is not appropriate for a long simulation with steady forcing, in any case.

What we do learn from the initial transients is that the circulation in the canyon reacts in a few days to an increase in the strength of surface stress. Over an additional few days, nonlinear effects modify the circulation, spreading the across shore flow over the canyon. Density advection reduces the pressure gradients over a week or so. In spite of these adjustments, upwelling in the canyon continues at rates that allow considerable water (20 mSv or 1.6 km^3 d^{-1}) to move onto the shelf. By continuity, there must be an equivalent transport of water off the shelf across the adjacent shelf break, flushing the continental shelf. If there were one canyon per 100 km of a shelf (100 m deep and 100 km wide), then steady upwelling would flush this shelf in about 2 years (1000 km^3 water volume over exchange of 2 km^3 d^{-1} gives 500 days).

5. Conclusions

This paper considers steady flow near and within a narrow submarine canyon driven by surface wind stress. The thermal and dynamic features in the solutions are consistent with the observations, which suggest that the ocean model can be used in a comprehensive canyon-shelf flow interaction study. On the basis of model results some unresolved issues in canyon dynamics are analyzed.

In the upper layers (above 100 m) the influence of canyon topography on the flow is gentle, with the effect being reduced as stratification increases. Alongshelf flow turns slightly onshore upstream of the canyon and turns offshore downstream. Near the rim (100-200 m), flow turns into the canyon mouth and moves across shore on the downstream side of the canyon. Upwelling or downwelling occurs near the canyon rim depending on the direction of the winds. A closed circulation is created within the canyon in response to vortex stretching (upwelling) or compression (downwelling). Upwelling winds create persistent across shelf transport, while downwelling winds lead to small net exchanges.

This picture is consistent with the previous observations, and we are able to deduce mechanisms that drive this circulation. With upwelling winds, onshore flow in the canyon is driven by the pressure gradient because of the tilted free surface and the reduction of alongshore flow by the canyon topography. The contrary baroclinic pressure gradient reduces but does not eliminate the surface pressure gradient so the force extends deep into the canyon. This mechanism does not depend on momentum advection. Cyclonic vorticity is produced by flow detachment from the upstream rim and by vortex stretching due to continual upwelling. Closed circulation in the canyon develops in response to these two processes. Downwelling winds produce oppositely directed circulation in the upper and middle layers. These circulation patterns develop in about a week but change slowly over an additional 2 weeks with continuous forcing.

This study has practical importance because it calculates the amount of the dense water transported to the continental shelf through submarine canyons, resulting in shelf flushing times of a few (2-5) years. There is also a rectification of this cross-shore transport as upwelling causes exchange but downwelling does not. Thus transports from reversing winds do not cancel, and canyon circulation can still flush the shelf even in cases of winds with zero mean. Better estimates of the flushing times are obtained with time variable winds, which will be considered in the following paper (Klinck *et al.*, submitted manuscript, 2000).

References

Allen, J. S., P. A. Newberger, and J. Fedriuk, Upwelling circulation on the Oregon continental shelf, part I, Response to idealized forcing, *J. Phys. Oceanogr.*, *25*, 1843-1866, 1995.

Allen, S. E., Topographically generated, subinertial flows within a finite length canyon, *J. Phys. Oceanogr.*, *26*, 1608-1632, 1996.

Barth, J. A., Stability of a coastal upwelling front, 2, Model results and comparison with observations, *J. Geophys. Res.*, *94*, 10,857-10,883, 1989.

Barth, J. A., Short-wavelength instability on coastal jets and fronts, *J. Geophys. Res.*, *99*, 16,095-16,115, 1994.

Beckmann, A., and D. B. Haidvogel, Numerical simulation of flow around a tall isolated sea mountain, part I, Problem formation and model accuracy, *J. Phys. Oceanogr.*, *23*, 1736-1753, 1993.

Chapman, D. C., and S. J. Lentz, Adjustment of stratified flow over a sloping bottom, *J. Phys. Oceanogr.*, *27*, 340-356, 1997.

Freeland, H. J., and K. L. Denman, A topographically controlled upwelling center off southern Vancouver Island, *J. Mar. Res.*, *40*, 1069-1093, 1982.

Haney, R. L., On the pressure gradient force over steep topography in sigma coordinate ocean models, *J. Phys. Oceanogr.*, *21*, 610-619, 1991.

Hickey, B. M., The response of a steep-sided, narrow canyon to time-variable wind forcing, *J. Phys. Oceanogr.*, *27*, 697-726, 1997.

Hickey, B. M., Coastal oceanography of western North America from the tip of Baja California to Vanouver Island, in *The Sea*, vol. 11, edited by A. R. Robinson and K. H. Brink, pp. 345-393, John Wiley, New York, 1998.

Holloway, G., Systematic forcing of large-scale geophysical flows by eddy-topography interaction, *J. Fluid Mech.*, *184*, 463-476, 1987.

Hunkins, K., Mean and tidal currents in Baltimore canyon, *J. Geophys. Res.*, *93*, 6917-6929, 1988.

Inman, D. L., C. E. Nordstrom, and R. E. Flick, Currents in submarine canyons: An air-sea-land interaction, *Annu. Rev. Fluid Mech.*, *8*, 275-310, 1976.

Klinck, J. M., The influence of a narrow transverse canyon on initially geostrophic flow, *J. Geophys. Res.*, *93*, 509-515, 1988.

Klinck, J. M., Geostrophic adjustment over submarine canyons, *J. Geophys. Res.*, *94*, 6133-6144, 1989.

Klinck, J. M., Circulation near submarine canyons: a modeling study, *J. Geophys. Res.*, *101*, 1211-1223, 1996.

Large, W. G., J. C. McWilliams, and S. C. Doney, Oceanic vertical mixing: A review and a model with nonlocal boundary layer parameterization, *Rev. Geophys.*, *32*, 363-403, 1994.

Mellor, G. L., T. Ezer, and L.-Y. Oey, The pressure gradient conundrum of sigma coordinate ocean models, *J. Atmos. Oceanic Technol.*, *11*, 1126-1134, 1994.

Middleton, J. F., and M. Cirano, Wind-forced downwelling slope currents: A numerical study, *J. Phys. Oceanogr.*, *29*, 1723-1743, 1999.

Song, Y., and D. B. Haidvogel, A semi-implicit ocean circulation model using a generalized topography-following coordinate system, *J. Comput. Phys*, *115*, 228-244, 1994.

J. M. Klinck Center for Coastal Physical Oceanography, Old Dominion University, Norfolk, VA 23529. (klinck@ccpo.odu.edu)

J. She, Danish Meteorological Institute, Copenhagen, Denmark.